Climate Dynamics
https://doi.org/10.1007/s00382-019-04769-2

Observed relationship between the Turkana low-level jet and boreal summer convection

Edward K. Vizy[1] · **Kerry H. Cook**[1]

Received: 14 January 2019 / Accepted: 9 April 2019

Abstract
The Turkana low-level jet is a circulation feature over northern Kenya that is not spatially well-resolved in many observational datasets. Here, high-resolution TRMM, IMERG, and CMORPH precipitation estimates, along with the ERA5 and MERRA2 reanalyses are analyzed to better understand the controls on jet strength and the relationship between the jet and boreal summer rainfall variability in the jet exit region over South Sudan. The height of the South Sudan wet season, August, is analyzed for 2000–2017. Climatologically, rainfall peaks over the jet exit region during the early morning hours, coinciding with the jet maximum. The strong jet enhances low-level wind convergence and briefly shifts the low-level zonal moisture gradient westward. Over the western South Sudan, rainfall peaks in the late afternoon/evening in association with daytime heating. The correlation between the daily Turkana Jet strength and precipitation indicates a significant negative relationship over eastern South Sudan, and over the Ethiopian and East African Highlands. Composite analysis of strong and weak jet periods reveal that the atmospheric conditions associated with a strong jet include enhanced low-level ridging along the East African coast south of the equator resulting in a stronger height gradient in the Turkana Channel, as well drier conditions over the channel and adjacent highlands. These conditions support a stronger jet that is further enhanced by katabatic flow due to the stronger nighttime cooling over the highlands, as well as enhanced dry air advection over the jet exit region. Thus, while low-level convergence may increase, convection weakens over eastern South Sudan due to the reduced atmospheric moisture content and weaker instability. The opposite occurs for the weak jet case.

Keywords Turkana low-level jet · East African rainfall · Kenya · South Sudan · Ethiopia · Diurnal cycle of rainfall · Rainfall variability · Katabatic winds · ERA5 · IMERG

1 Introduction

Eastern Africa, which includes Sudan, Eritrea, Ethiopia, Djibouti, Somalia, Kenya, South Sudan, Uganda, Tanzania, and Rwanda, is sensitive to weather and climate fluctuations across multiple timescales. The region is prone to devastating droughts such as the Ethiopian drought of the mid-1980s and the East African drought of 2011, the latter being the most severe of the past 60 years, affecting more than 12 million people. In many cases, the impacts of drought are thought to be related to regional conflict that exacerbates food shortages and famine (ReliefWeb 2017; Lu 2018). For example, parts of South Sudan have been experiencing famine conditions since 2017 due not only to drought and poor crop yields, but also the effects of the ongoing civil war. Given East Africa's strong reliance on rainfed agriculture practices for food security, it is crucial to improve our understanding of the physical processes that control the region's rainfall.

While there has been some progress made in identifying the influence of the Turkana low-level jet on regional aridity (Nicholson 2016), our current understanding of weather and climate variability over Eastern Africa is limited due to several factors. One issue is the scarcity of ground-based observations, especially over remote continental interior areas west of the Ethiopian and East African Highlands, which limits the opportunity to ground-truth satellite and reanalysis products. Another issue is the complex terrain. The Ethiopian Highlands, East African Highlands of Kenya and Tanzania, and the Turkana Channel, which is a narrow

✉ Edward K. Vizy
ned@jsg.utexas.edu

[1] Department of Geological Sciences, Jackson School of Geosciences, The University of Texas at Austin, Austin, TX 78712, USA

Published online: 13 April 2019

gap between the two Highlands over northwestern Kenya (Fig. 1), are not well resolved at the spatial resolutions of many atmospheric models used for weather/climate prediction. However, the recent availability of high spatio-temporal resolution satellite-derived precipitation estimates from NOAA's Climate Prediction Center morphing technique precipitation product (CMORPH; Joyce et al. 2004) and NASA's Integrated Multi-satellite Retrievals for GPM (IMERG; Huffman et al. 2014) along with the ECMWF ERA5 reanalysis output (ERA5 2018), afford the opportunity to refine our understanding of Eastern African rainfall variability at the necessary spatio-temporal scales.

The purpose of this study is to improve our understanding of the relationship between the Turkana Jet and the diurnal cycle of boreal summer rainfall in the vicinity of the jet exit region over continental interior Eastern Africa (South Sudan). More specifically, we want to take advantage of the recently available, high-resolution precipitation and atmospheric reanalysis datasets to refine our understanding of the structure and variability of the Turkana Jet. This includes better understanding the atmospheric conditions associated with strong and weak jet periods, and the relationship between the jet strength and regional rainfall during the height of the jet exit region's primary wet season (August) on synoptic to diurnal timescales.

Background on the Turkana Jet and Eastern African climate variability is provided in Sect. 2. The observational datasets analyzed are discussed in Sect. 3. Results are presented in Sect. 4, while conclusions are summarized in Sect. 5.

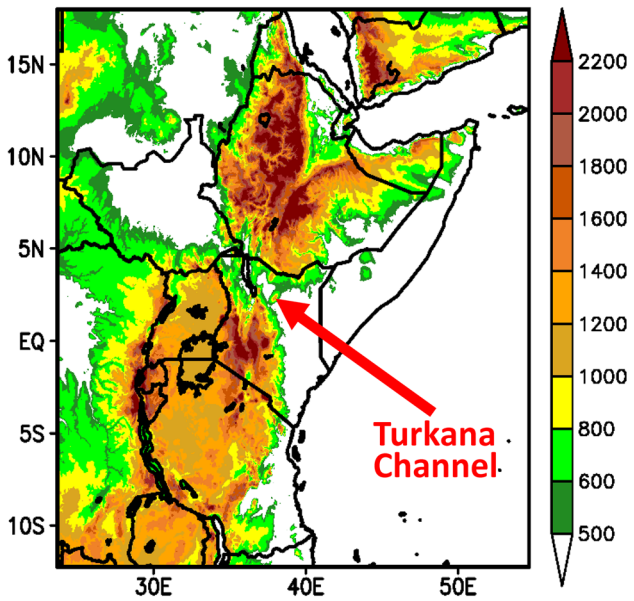

Fig. 1 East African topography (m) resolved at 2-minute (~4 km) resolution from USGS DEM

2 Background

Figure 1 shows the topography of Eastern Africa. The region ranges from low-lying coastal plains of Somalia, Kenya, and Tanzania, to the mountains of the Ethiopian and East African Highlands, with peaks ranging up to 4550 m (i.e., Ras Dashen) and 5895 m (i.e., Mount Kilimanjaro), respectively. The coastal plain itself is narrow south of the equator (around 100 km or less), but widens considerably north of the equator (> 500 km). Numerous Rift valley lakes are located among the highland valleys, including Lakes Victoria, Turkana, Albert, Kyoga, Abaya, and Tana. Separating the Ethiopian and East African Highlands is the Turkana Channel, a relatively low-lying valley with a southeast-to-northwest orientation from the coastal plains of Kenya to South Sudan.

The seasonality of rainfall over Eastern Africa is equally as complex as the topography. A number of past studies (e.g., Griffith 1972; Nicholson 1996, 1998, 2000) have classified rainfall seasonality over Eastern Africa based primarily on in-situ and rain gauge data. More recently, Herrmann and Mohr (2011) classified Eastern African rainfall seasonality using TRMM gridded satellite-derived rainfall estimates. Inspection of such classification maps [e.g., see Fig. 1 from Herrmann and Mohr (2011)] reveals the intricate nature of the seasonality of precipitation over the region. For example, the coastal plains of Kenya, western Somalia, and southern Ethiopia have two distinct wet seasons, while interior areas such as northern Ethiopia, Sudan, and South Sudan have a single wet season. This is confirmed in Fig. 2, which shows the climatological seasonality of rainfall on each side of the Turkana Channel from various satellite-derived observations and atmospheric reanalyses. Consistent with Herrmann and Mohr (2011), a single rainfall peak occurs during the boreal summer in the Turkana Jet exit region over South Sudan (Fig. 2a), while boreal spring and late boreal fall rainfall peaks occur over Kenyan coastal plains in the jet entrance region (Fig. 2b).

The low-level circulation along the East African coast is strongly tied to the seasonality of the Indian Monsoon system. Around mid-May Southern Hemisphere-to-Northern Hemisphere cross-equatorial low-level jet (a.k.a. the East African low-level jet or Somali Jet) forms and lasts through September. This flow follows the coast as it crosses the equator before turning eastward of the Somali Coast directed towards India. During the winter months this pattern reverses direction. The Somali Jet was first identified by Bunker (1965) and Findlater (1966) and has been subsequently studied (Krishnamurti et al. 1976; Anderson 1976; Findlater 1977; Hart 1977; Hart et al. 1978; Bannon 1979) to better understand its development

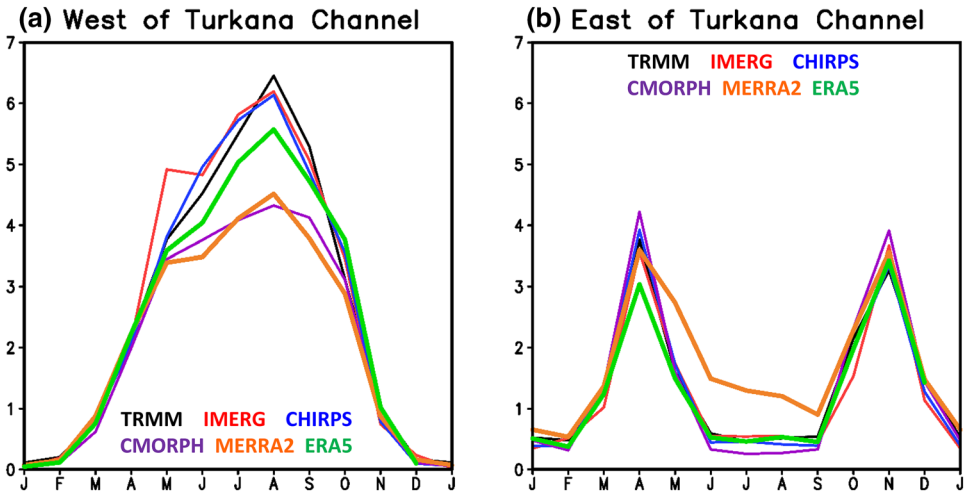

Fig. 2 Climatological monthly mean precipitation (mm day^{-1}) area-averaged over the Turkana Jet **a** exit (25°E–34°E; 5°N–10°N), and **b** entrance (36°E–42°E; 2°S–5°N) regions for the TRMM TMPA (black), IMERG (red), CHIRPS (blue), and CMORPH datasets, and MERRA2, and ERA5 reanalyses. All climatologies are calculated from 2000–2017 except IMERG, which is 2014–2017

and maintenance. The jet core typically lies around 1–1.5 km above the surface (Findlater 1969) and provides an estimated 65% of the global low-level cross-equatorial mass flux transport (Rodwell and Hoskins 1995). While this jet has been linked to the Indian monsoon system (Krishnamurti et al. 1976; Bannon 1979), the highlands of East Africa play an integral role in its intensification and confinement along the coast (Krishnamurti et al. 1976; Ngara and Asnani 1978; Rodwell and Hoskins 1995).

During the solstitial months, rainfall over the equatorial East African coastal plains is limited (Fig. 2b) as the low-level cross-equatorial jet is strong and flow is divergent (Trewartha 1981; Nicholson 1996; Hartman 2018). As a result, highest rainfall rates occur during the transition seasons (Sun et al. 1999; Indeje et al. 2001; Riddle and Cook 2008), from March to May (termed the long-rains) and October to December (the short rains). Given the importance of rainfall for agricultural needs and the high variability of rainfall over the coastal plains region of Somalia, Kenya, and Tanzania, more attention from the scientific community is generally directed at understanding rainfall variability during the long-rains and short-rains periods (e.g., Cook and Vizy 2012, 2013; Lyon and Dewitt 2012; Liebmann et al. 2014; Rowell et al. 2015).

Compared to the equatorial coastal plains of East Africa, our understanding of rainfall over the continental interior of Eastern Africa west of the highlands is more limited. Rainfall occurs here during the boreal summer (Fig. 2a), coinciding with the peak of the West African summer monsoon. Past studies (Mekonnen et al. 2008; Mekonnen and Thorncroft 2016; Levin et al. 2009; Williams et al. 2012) indicate that during the boreal summer moisture transport from the equatorial Congo is crucial for the development of convection over and to the west of the Ethiopian Highlands. Thus, there is relationship between the equatorial Congo region and the South Sudan/Ethiopian Highlands, with enhanced convection in the former preceding convection in the latter tied to the propagation of convectively-coupled Kelvin waves (Mekonnen et al. 2008, 2016).

Connecting the continental interior Eastern Africa with the coastal Kenyan plains is a prominent low-level jet feature, the Turkana jet. The Turkana jet is smaller in scale than the Somali Jet, and its role in regional weather/climate variability is not well understood. Kinuthia and Asnani (1982) and Kinuthia (1992) first documented its existence using pilot balloon observations. They observed that this southeasterly low-level jet can vary in strength, with wind speeds exceeding 50 m s^{-1} in some instances. The jet strength varies throughout the channel, with stronger speeds where the channel is narrow.

Nicholson's (2016) analysis of the 0.75°-resolution, 6-hourly ERA-Interim (Dee et al. 2011) atmospheric reanalysis data and TRMM TMPA satellite-derived rainfall estimates (Huffman et al. 2007) provides a more detailed climatological view of the Turkana jet. While the jet is present year-round, it is strongest during the boreal summer months of June–September. The jet is strongest between 00 and 06Z, and weakest near 12Z. Nicholson (2016) also suggests a relationship between the jet strength and rainfall, especially during the nighttime hours, with a strong jet associated with reduced rainfall. Nicholson (2016) also suggests a connection between rainfall and the regional vertical motion field, however the robustness of these results may be dependent upon the spatio-temporal resolution of the ERA-Interim reanalysis analyzed. More work is still needed to understand this relationship, especially in regards to the role of the topography of the region.

A few studies have examined interactions between large-scale and mesoscale processes associated with the low-level flow over the Turkana Channel. Mukabana and Pielke (1996) show in their modeling study that the topography of the highlands has a significant impact on the diurnal cycle of

the circulation and precipitation in a case study during the long-rains. Differential heating between the elevated terrain and the low-lying coastal plain/Turkana Channel valley can incite diurnal katabatic-anabatic flow which may affect the jet strength. Sun et al. (1999) discuss an improved simulation of the East African short-rains, including the seasonal evolution of the Turkana Jet and the development of low-level divergence in the channel, in higher resolution regional modeling that better represents land surface conditions in the region. Indeje et al. (2001) examine the kinematics of the Turkana Jet during the short rains (October–December). Their results indicate that the Turkana Jet is largely dependent upon topography, with orographic forcing being the most important factor on the strength of the jet while the depth and the width of the channel help to determine the vertical structure and location of the jet. Furthermore, Indeje et al. (2001) found that more localized thermal and frictional forcing are just as influential as large-scale forcing in the development and maintenance of the jet. This suggests that the heating of the highlands adjacent to the Turkana Channel can be an important factor for the variability of this jet. More recently, Hartman's (2018) analysis of NCEP CFSR and MERRA reanalysis data suggests that the thermal forcing in and around the Turkana Channel is likely the most important factor controlling the strength of the Turkana Jet. Overall, these studies indicate that both large-scale and mesoscale processes need to be considered when trying to understand Turkana Jet variability and its impact on regional rainfall variability.

3 Observational datasets and atmospheric reanalyses

Datasets and reanalyses that provide high spatio-temporal resolution are needed to resolve the diurnal cycle of rainfall and the Turkana jet. Each dataset is discussed briefly below.

For rainfall, the following four datasets are evaluated:

- NASA TRMM Multi-satellite Precipitation analysis (TRMM; Huffman et al. 2007)—this product blends available microwave and IR satellite estimates to create a 3-hourly rainfall product at a spatial resolution of 0.25°. While TRMM is the coarsest resolution of the four precipitation datasets analyzed here, it does have a lengthy record (1998–present). TRMM is used here to evaluate the diurnal cycle of rainfall, evaluate the extent to which it is represented in the atmospheric reanalyses, and formulate composites.
- Climate Hazards group InfraRed Precipitation with Stations (CHIRPS; Funk et al. 2015)—this product provides 0.1° resolution monthly rainfall estimates over land from 1981–present. CHIRPS blends 0.05° resolution satellite imagery with in-situ measurements to produce a gridded monthly time series of rainfall. This dataset is primarily used to evaluate the climatological monthly rainfall by comparing with the other rainfall datasets in addition to the atmospheric reanalyses.
- NOAA Climate Prediction Center Morphing Technique Precipitation V2 biased-corrected estimate (CMORPH; Xie et al. 2017)—this 8-km resolution dataset produces 30-minute estimates of rainfall from 1998–present by using rainfall estimates from passive microwave observations and extrapolating them backwards and forwards in time via spatial propagation information obtained from geostationary IR satellite data. Similar to TRMM, CMORPH is used to evaluate the diurnal cycle of rainfall, evaluate the atmospheric reanalyses, and formulate composites.
- NASA Integrated Multi-satellite Retrievals for Global Precipitation Measurement (IMERG; Huffman et al. 2014)—IMERG is the next generation of TRMM and provides global 0.1° resolution 30-min rainfall estimates using satellite retrievals from network of global satellites. As such, the record length of this product is shorter than TRMM and CMORPH (2014–present). Here, IMERG is used to evaluate the diurnal cycle of rainfall and compare with the other datasets and atmospheric reanalyses. Dezfuli et al. (2017) demonstrated that, when compared to station data over East Africa (one station in Kenya), IMERG does improve on the representation of the diurnal cycle of rainfall compared to TRMM.

Two state-of-the-art atmospheric reanalyses are utilized to evaluate the local and regional environmental and atmospheric circulation conditions associated with the diurnal cycle of rainfall in the jet exit region, and understand the relationship between the diurnal cycle or rainfall and the Turkana jet. They are:

- ECMWF ERA5 reanalysis (ERA5; ERA5 2018)—ERA5 is the newest atmospheric reanalysis product available from ECMWF. ERA5 provides global 0.25° resolution hourly gridded output of surface and atmospheric fields, ideal for evaluating the diurnal cycle of rainfall as well as small-scale features such as the Turkana jet. At the time this study was conducted data were available from 2000–2017.
- NASA Modern-Era Retrospective analysis for Research and Applications, Version 2 (MERRA2; Gelaro et al. 2017)—MERRA2 provides 3-hourly estimates of upper-air fields and hourly estimates of some surface fields including precipitation at 0.625° longitude × 0.5° latitude spatial resolutions from 1980–present. While the spatial resolution of MERRA2 is comparable to other reanalyses such as ERAI (Dee et al. 2011) that have been used to

better understand the Turkana Jet (Nicholson 2016), its 3-hourly temporal resolution is better suited to evaluate the diurnal nature of the jet compared to ERAI and JRA-55 (Kobayashi et al. 2015).

4 Results

4.1 Climatological analysis

To refine our understanding of the structure of the Turkana Jet and the jet's relationship to regional rainfall, climatological August conditions over the Turkana Jet channel and jet exit region are first analyzed for the various high-resolution observational and atmospheric reanalysis datasets selected (see Sect. 3). A common climatological period of 2000–2017 (18 years) is utilized for all atmospheric reanalyses and rainfall datasets except for IMERG, for which the climatology is formulated over 2014–2017 due to its shorter record length.

Figure 3 shows the resolved topography and vertical cross-sections of the climatological August mean wind speed cutting across and parallel to the Turkana Channel axis of orientation from ERA5 (Fig. 3a–d) and MERRA2 (Fig. 3e–h). The channel is relatively flat, with lowest elevations over Lake Turkana. Compared with the coarser resolution of MERRA2 (Fig. 3e), features such as Mount Nyiru (2.1°N; 36.8°), Mount Marsabit (2.3°N; 37.9°E), and the Huri Hills (3.5°N; 37.8°E) are more distinguishable in the entrance of the channel, and the topography of the channel walls emerges in the 0.25° resolution ERA5 (Fig. 3a).

The red transect crosses the channel at the western exit region of the channel at A1–A2, while the blue transect crosses the narrowest point of the channel at B1–B2. At the exit region, the jet core has a magnitude of around 7 m s^{-1} between 900 and 850 hPa in ERA5 (Fig. 3b). The jet core is weaker and wider in the coarser resolution MERRA2 (Fig. 3f). At B1–B2 the jet core is stronger, with magnitudes around 11 m s^{-1} in ERA5 (Fig. 3c) and 12 m s^{-1} in MERRA2 (Fig. 3g). The core is extends from 900 hPa to about 850 hPa in the higher resolution ERA5, while from 925 hPa to around 850 hPa in MERRA2.

Examination of the vertical transects parallel to the Turkana Channel in ERA5 (Fig. 3d) and MERRA2 (Fig. 3h) indicate differences in the structure of the jet between the two reanalyses. In the coarser resolution MERRA2, the jet core is positioned around 900 hPa with the strongest wind speeds (13–14 m s^{-1}) in the entrance region, decaying to the northwest toward the exit region. While to first order ERA5 has a similar jet core structure, the jet strength is more variable with a maximum of 13 m s^{-1} in the entrance region, and a secondary maximum of 11 m s^{-1} around 37°E where

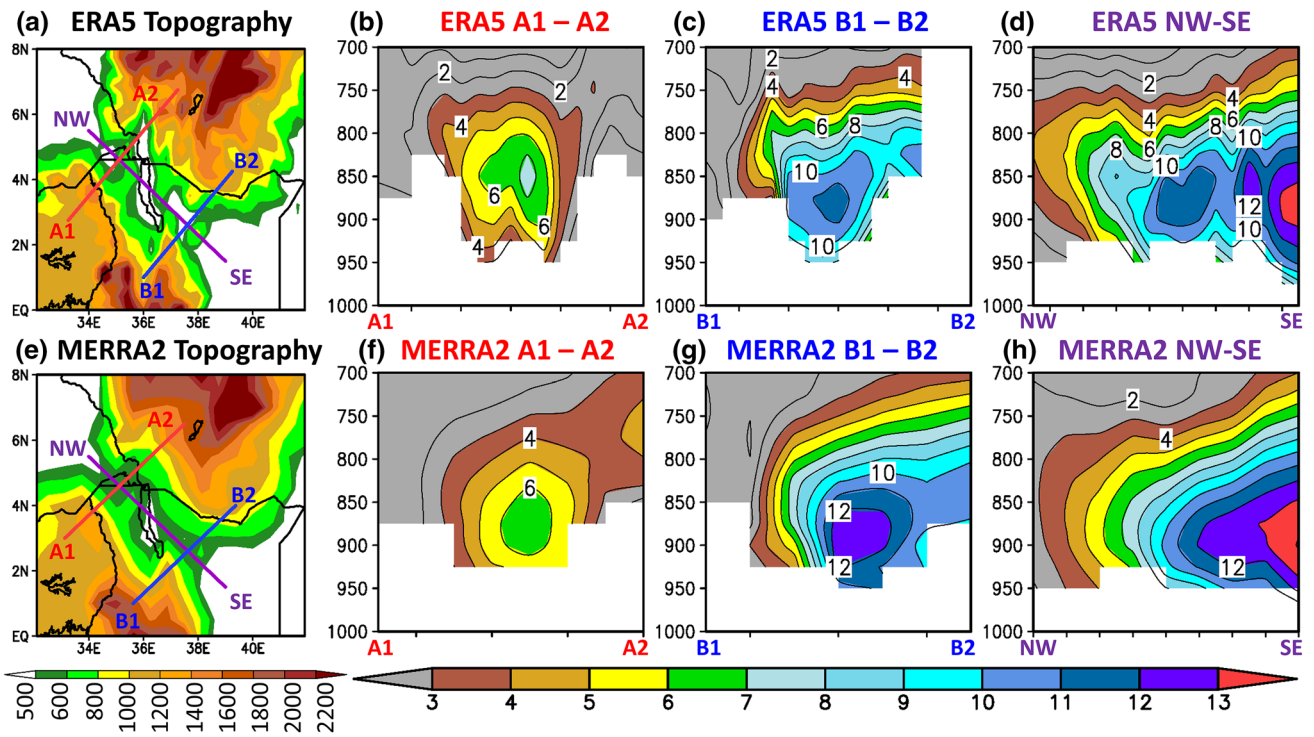

Fig. 3 ERA5 **a** Topography (m) and location of analysis transects, and the 2000–2017 climatological August surface—700 hPa wind speed (m s^{-1}) vertical transects at **b** A1–A2, **c** B1–B2, and **d** parallel to the Turkana Channel at NW–SE. **e–h** shows the same fields as **a–d**, respectively, but for MERRA2

the channel is most narrow. This structure is consistent with the climatological structure found in the NCEP CFSR reanalysis (Hartman 2018). Given that ERA5 better resolves the Turkana Channel, it is more likely that the jet is variable in strength in the channel as suggested by Fig. 3d. Furthermore, jet magnitudes in the channel in both reanalyses fall within the range of the observed pilot-balloon jet strength estimates made by Kinuthia (1992) giving us some confidence that they are realistically capturing the Turkana Jet strength. However, without additional observational data at different locations in the channel we cannot conclude with certainty the extent to which ERA5 is realistic, so some caution needs to be taken when interpreting results.

Figure 4 shows the 900 hPa climatological August geopotential heights and wind speeds in the Turkana Channel for ERA5 (Fig. 4a) and MERRA2 (Fig. 4b). Both reanalyses indicate a strong low-level height gradient across the channel with lower heights in the jet exit region to the west, and higher heights in the entrance region to the east. As observed in Fig. 3, the jet core is stronger in the channel in MERRA2 compared to ERA5. The strong height gradient across the channel is consistent with the Bernoulli effect as discussed in the literature (Indeje et al. 2001) as flow is directed down the height gradient from higher to lower heights through the channel.

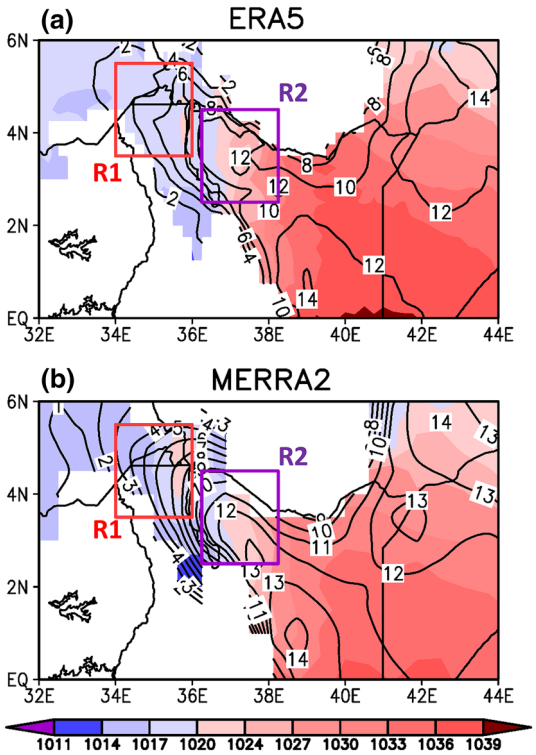

Fig. 4 Climatological August monthly 900 hPa geopotential heights (shaded; m) and wind speed (contours; m s^{-1}) for **a** ERA5, and **b** MERRA2 reanalyses. The R1 (red) and R2 (purple) boxes are the averaging regions used for the subsequent analysis to represent the Turkana jet exit and maximum wind speed regions, respectively

Figure 5 shows the climatological August monthly mean precipitation from 4 different observational/satellite-derived datasets (Fig. 5a–d) and the two atmospheric reanalyses (Fig. 5e, f). All datasets are shown on their native grids to preserve information, with the estimated spatial resolution of each provided. Overall, the observations are in good agreement that the largest August rainfall rates are located over the Ethiopian Highlands. All the datasets also indicate heavier rainfall rates (> 4 mm day^{-1}) to the north and east of Lake Victoria, and minimal rainfall (< 1 mm day^{-1}) along the coastal plains of Somalia, Kenya, and Tanzania. To the west of the Ethiopian and East African Highlands, the agreement among the datasets is not as strong. For example, over the eastern Congo Basin just west of Rwanda, each dataset produces a rainfall maximum, but magnitudes range from 6 mm day^{-1} in TRMM (Fig. 5a) to over 15 mm day^{-1} in CMORPH (Fig. 5b). The lack of agreement is likely the result of a sparser gauge network in this region. There are also differences over Sudan and South Sudan, with TRMM, IMERG, and CHIRPS indicating a maximum over the northern South Sudan up to 7 mm day^{-1}, while CMORPH has lower rainfall rates of 2–4 mm day^{-1}. Additionally, all four observational datasets indicate that there is minimal rainfall over the Turkana Channel. This is consistent with daily station data from Lodwar, Kenya (3.11°N; 35.61°E) west of Lake Turkana (not shown).

Figure 5e, f show the climatological August monthly mean rainfall from ERA5 and MERRA2, respectively, to evaluate the extent to which the reanalyses capture the observed rainfall patterns. Overall, both reanalyses yield a spatial distribution of rainfall similar to the observations, including maxima over the Ethiopian Highlands, near Lake Victoria, over the eastern Congo Basin, and over central and northern South Sudan. Maxima magnitudes over the elevated terrain of Ethiopia and surrounding Lake Victoria are generally larger than in the observations. Both ERA5 and MERRA2 yield light rainfall along the coasts of Somalia, Kenya, and Tanzania that extends eastward over the western Indian Ocean that is more spatially robust compared to the observations. We can conclude from Fig. 5 that ERA5 and MERRA2 produce the observed August monthly rainfall spatial distribution over Eastern Africa with reasonable accuracy, however there is less agreement on the rainfall intensity.

It is important to note that the Turkana Jet does not directly influence rainfall everywhere shown in Fig. 5. Based on Fig. 3d, h, and consistent with Nicholson (2016), the westward extent of the Turkana Jet extends only to about 33°E between 4°N–7°N in the reanalyses. Thus, the Turkana Jet's direct regional influence on rainfall is limited to the Turkana Channel of northern Kenya and southern Ethiopia,

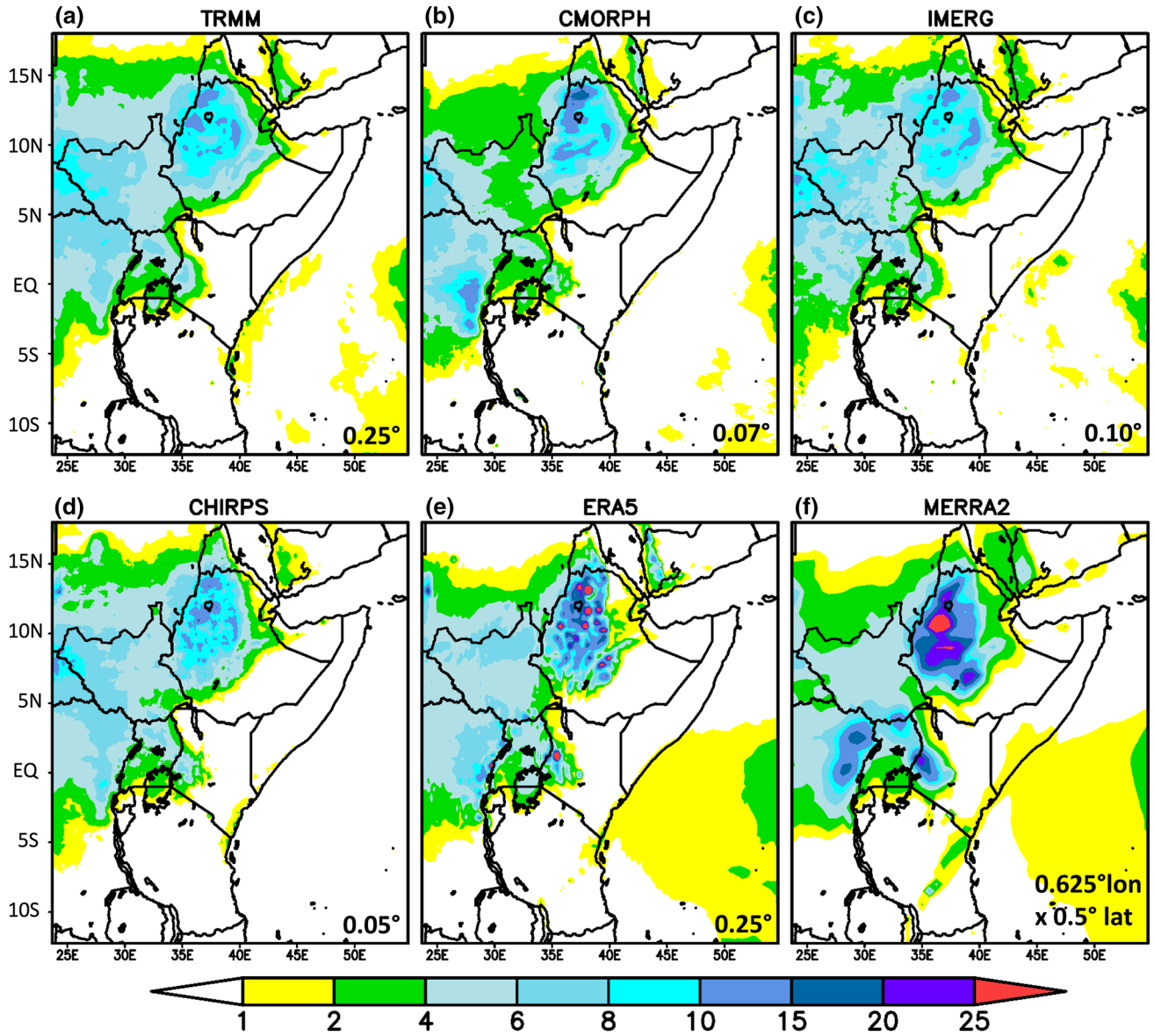

Fig. 5 Climatological August monthly precipitation (mm day^{-1}) for **a** TRMM, **b** CMORPH, **c** IMERG, and **d** CHIRPS datasets, and the **e** ERA5 and **f** MERRA2 reanalyses. The approximate spatial resolution of each dataset is provided in the lower right corner. All climatologies are calculated from 2000–2017 except IMERG, which is 2014–2017

as well as the southeastern South Sudan. We focus our climatological diurnal analysis below on this area to improve our understanding of the nature of the relationship between the jet and convection.

Figure 6 shows the climatological August diurnal cycle of precipitation between 35°E (Turkana Channel exit region) and 28°E (eastern South Sudan) averaged between 5°N–6.5°N for the satellite-derived observational datasets. TRMM (Fig. 6a) shows a distinct diurnal cycle of rainfall with enhanced morning convection of over 6 mm day^{-1} between 33–35°E that slowly propagates westward until 12Z. After 12Z, convection is strong generally west of 32°E and propagates westward through the rest of the day. This is associated with the development of afternoon convection associated with daytime heating over the central and western South Sudan. East of 32°E rainfall generally diminishes from 12Z to 00Z.

CMORPH and IMERG exhibit a similar climatological diurnal cycle of rainfall as TRMM. In the case of CMORPH (Fig. 6b), morning rainfall rates before 12Z east of 32°E are slightly higher, while afternoon rainfall rates west of 32°E are generally lower than TRMM. For IMERG (Fig. 6c), rainfall rates are higher both in the morning east of 32°E, and after 12Z west of 32°E. Furthermore, IMERG suggests that

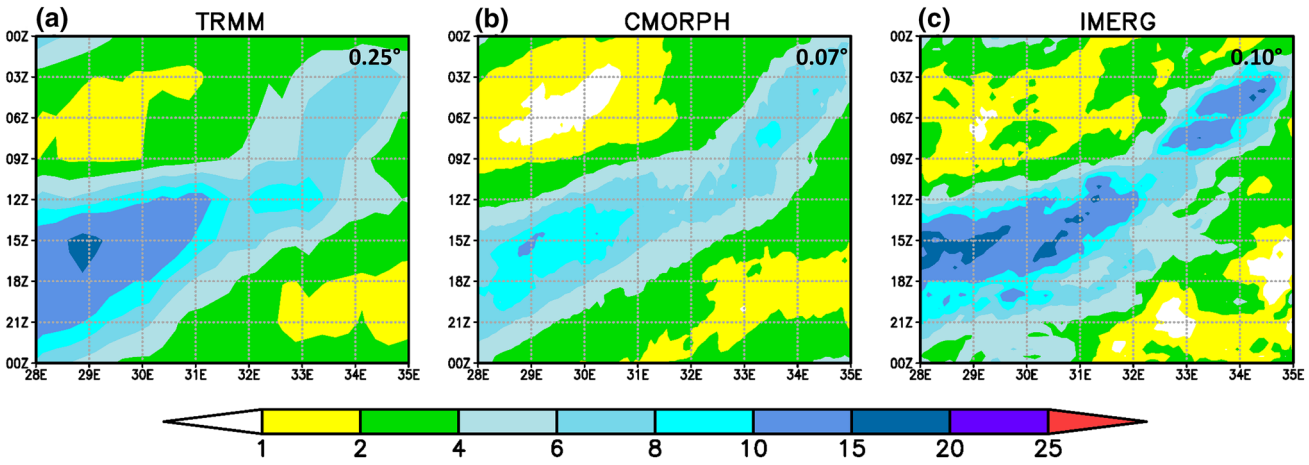

Fig. 6 Climatological August diurnal cycle of precipitation (mm day^{-1}) averaged between 5°N–6.5°N for the **a** TRMM TMPA, **b** CMORPH, and **c** IMERG datasets. All climatologies are calculated from 2000–2017 except IMERG, which is 2014–2017

the afternoon propagation of the heaviest rainfall greater than 10 mm day^{-1} is shorter in duration, lasting between 12Z–18Z rather than 12Z–21Z as is the case for TRMM and CMORPH. This difference may be due to the shorter climatological averaging period for IMERG.

Figure 7a shows the climatological diurnal cycle of rainfall along with the 900 hPa wind speed averaged between 5°N–6.5°N for ERA5. To first order, ERA5 does capture the observed diurnal cycle of rainfall including the morning maximum following local sunrise between 3Z–9Z east of 32°E, and the broader afternoon maximum after 12Z west of 32°E with peak rainfall rates around 15Z at local sunset. Interestingly, the afternoon maximum more closely resembles IMERG with the westward propagation being shorter lived, but the afternoon propagation of the convective systems appears to be lacking in ERA5. In terms of low-level wind speeds, the morning maximum in rainfall coincides with a westward extension to 33°E and strengthening of the Turkana Jet, as climatological magnitudes of the jet are greater than 5 m s^{-1} compared to less than 4 m s^{-1} between 12Z–15Z. In the evening after 15Z, the Turkana jet strengthens again.

Unlike ERA5, MERRA2 (Fig. 7b) does not capture the climatological diurnal cycle of rainfall very well. Instead, there is a maximum across the entire region shown between 3Z–12Z, then lower rainfall rates after 12Z. While MERRA2 does indicate a morning extension and intensification of the Turkana Jet to about 33°E, it is followed by relatively weak low-level winds less than 3 m s^{-1} after 12Z in contrast to ERA5.

The Turkana Jet is influential for the development of convection over eastern South Sudan. Figure 7c shows the ERA5 climatological diurnal cycle of 900 hPa wind convergence (shaded) and specific humidity (contours). Note, positive (negative) shaded values indicate wind convergence (divergence). Generally, low-level mixing ratio values are higher west of the Turkana Channel compared to over the channel and in the jet entrance region in Kenya regardless of the time of day during August. Thus, the jet is associated with the advection of relatively drier air via the channel into the eastern South Sudan, which is reflected in the diurnal cycle of specific humidity in ERA5 (Fig. 7c). This suggests the low-level moisture source for rainfall over South Sudan in August is equatorial Africa and not directly the Indian Ocean via low-level flow through the Turkana Channel. West of 33°E, the low-level moisture content is greater than 13 g kg^{-1} for the entire diurnal cycle, suggesting that there is ample low-level moisture available for convection over the entire day. East of 33°E, there is a gradual increase in low-level moisture content overnight. At 06Z there is an abrupt drying of the lower atmosphere that coincides with the jet maximum, followed by an equally abrupt increase in low-level moisture content between 06Z–09Z as the jet maximum weakens. After 09Z, there is more gradual low-level drying of the atmosphere for the rest of the day. The morning peak in rainfall in ERA5 (see Fig. 7a) coincides with when there is enhanced low-level wind convergence associated with the early morning strengthening of the Turkana Jet. This suggests that the low-level convergence in the exit region is a triggering mechanism for convection over the southeastern Sudan in the early morning provided that there is an ample supply of moisture/instability. This is followed by afternoon low-level divergence between 09Z–15Z, and then evening low-level convergence as the wind speeds intensify once again.

Figure 7d shows the same fields, but for MERRA2. The 900 hPa specific humidity east of 33°E exhibits a similar diurnal cycle as ERA5, albeit the low-level moisture content of the atmosphere appears to be 1–2 g kg^{-1} lower than ERA5, and there is no evidence of the brief period of drying

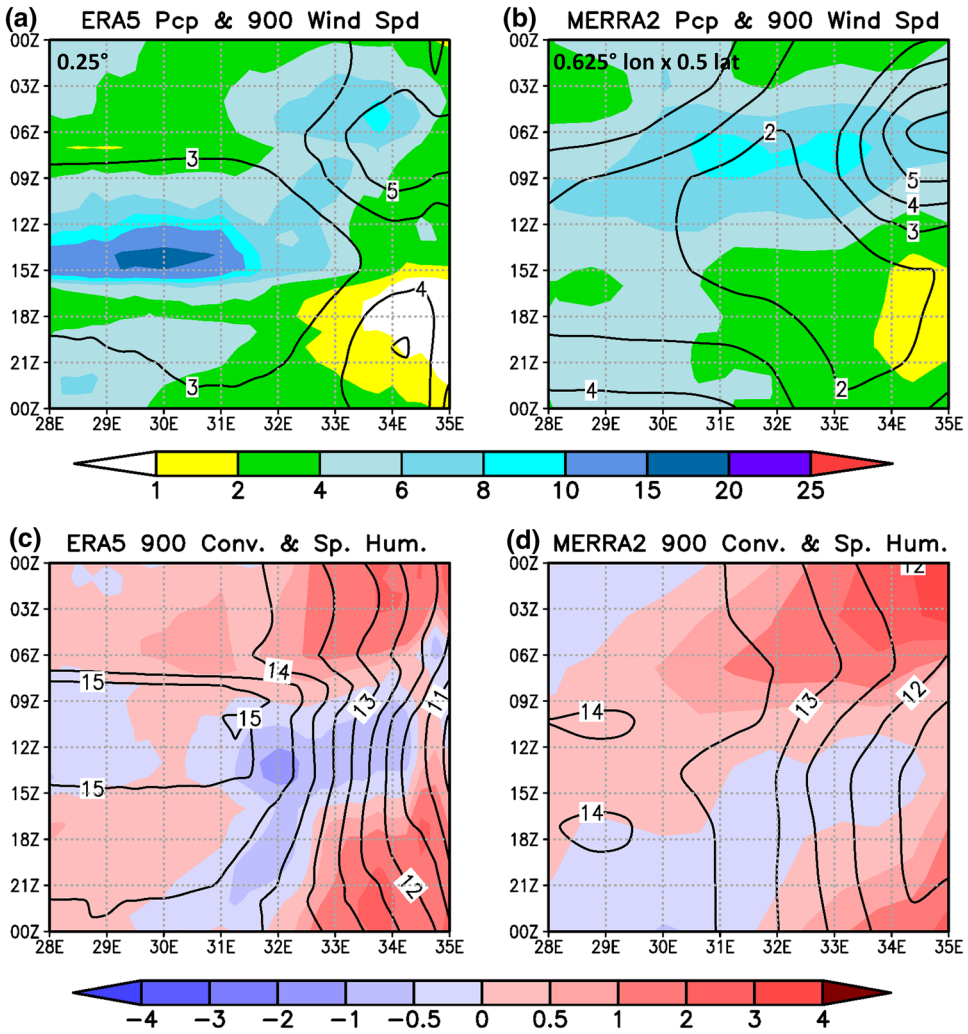

Fig. 7 **a** ERA5 and **b** MERRA2 2000–2017 climatological August diurnal cycle of precipitation (shaded; mm day^{-1}) and the 900 hPa wind speed (contour; m s^{-1}) averaged between 5°N–6.5°N. **c** ERA5 and **d** MERRA2 2000–2017 climatological August diurnal cycle of 900 hPa wind convergence (shaded; $\times 10^{-5}$ s^{-1}) and the 900 hPa specific humidity (contour; g kg^{-1}) averaged between 5°N–6.5°N

around 6Z associated with when the Turkana jet is maximum. This discrepancy may be due to the differences in the temporal resolutions between MERRA2 (3 hourly) and ERA5 (hourly), or related to the Turkana jet not extending as far west in MERRA2 as it does in ERA5. Morning convection in MERRA2 is also found to be related to strong low-level wind convergence associated with the nighttime intensification of the Turkana jet, however the evening wind convergence is weaker as the jet is slower to intensify east of 33°E compared to ERA5.

To better understand the differences between ERA5 and MERRA2, the diurnal cycle of the Turkana Jet for the R1 and R2 averaging regions of Fig. 4 are shown in Fig. 8a. R1 is located near the channel exit region where the jet strength is weakening, while R2 is located towards the entrance of the channel where the channel is narrowest. For R2 the 900 hPa wind speed is area-averaged over 2.5°N–4.5°N and 36.25°E–38.25°E, while for R1 it is area-averaged over 3.5°N–5.5°N and 34°E–36°E. In R2, both ERA5 and MERRA2 have fairly similar diurnal cycles. The most notable difference is that the nighttime jet maximum is 2–3 m s^{-1} stronger in MERRA2. For the jet exit region, R1, the diurnal amplitude of the jet is generally not as large as it is for the entrance region, however it is larger in MERRA2 as wind speeds between 15Z–21Z are slower to increase in the evening compared to ERA5.

Figure 8b shows an estimate of the 900 hPa climatological August diurnal cycle Turkana channel height gradient for the two reanalyses. Here, area-averaged 900 hPa heights from R1 and R2 are differenced to approximate the gradient across the channel. Both ERA5 and MERRA2 indicate the height gradient, hence the pressure gradient, is strongest at nighttime (15Z–07Z). During the day the height difference decreases by 50% or more, depending on the reanalysis and time of day. This coincides with when the jet weakens (Fig. 8a). The daytime reduction in the gradient is larger, and lasts longer in MERRA2 compared to ERA5.

A closer examination of how well the Turkana Channel is resolved in the two reanalyses explains some of the above-mentioned differences. Figure 8c shows a

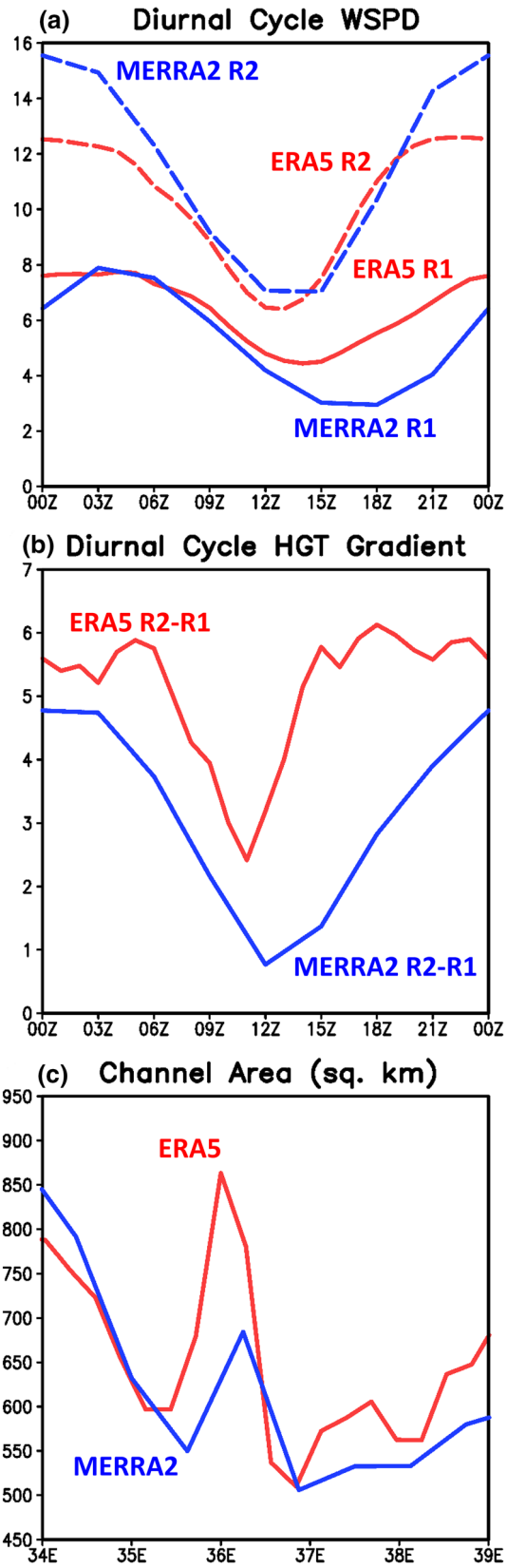

Fig. 8 2000–2017 ERA5 (red) and MERRA2 (blue) climatological August diurnal cycle of **a** 900 hPa wind speed (m s^{-1}) area-averaged over R1 (solid lines; 3.5°N–5.5°N and 34°E–36°E) and R2 (dashed lines; 2.5°N–4.5°N and 36.25°E–38.25°E), and **b** 900 hPa R2–R1 height difference. **c** Turkana Channel area estimated 825 hPa to the surface area (sq. km) for a given longitude for ERA5 and MERRA2

longitudinal cross-section of the estimated area from the surface to 825 hPa of the Turkana Channel in ERA5 and MERRA2. In the entrance region east of 36.25°E, we find that the resolved Turkana Channel is consistently narrower in MERRA2, likely helping to explain the stronger jet maximum in MERRA2. Namely, as the topography narrows and further constrains the low-level flow in the entrance region in MERRA2, the velocity of the low-level flow increases via the Bernoulli effect as there is also an associated drop in pressure (Indeje et al. 2001). Conversely, in the exit region there are greater differences in the resolved channel area. For example, MERRA2 does not widen as much as ERA5 in the vicinity of Lake Turkana (36°E), while west of 35°E, the areal-width of the channel is greater compared to ERA5. While it is difficult to interpret from MERRA2 due to its relatively coarse spatial and temporal resolutions, it would not be surprising if these area differences at least partially explain the delayed evening development of the Turkana jet in the exit region as the pressure gradient between the entrance and exit region (Fig. 8b) and the katabatic flows which may support the jet are likely weaker and/or slower to develop in MERRA2. These findings are also broadly consistent with the findings from Nicholson (2016) who analyzed the Turkana Jet in the 6-hourly 0.75° resolution ERA-Interim reanalysis. Furthermore, downslope katabatic flow is difficult to discern in ERA-Interim due to the relative spatio-temporal coarseness of this reanalysis [see Fig. 12 in Nicholson (2016)].

4.2 Turkana jet variability and regional rainfall

To further examine the relationship between the jet variability and regional rainfall, we form a Turkana Jet strength index using ERA5 by area-averaging the daily 900-hPa wind speed over the jet exit averaging region R1 shown in Fig. 4 and indicated by the red box in Fig. 9. This jet index is then correlated to daily precipitation from the observations and ERA5 output to identify areas where there is a significant relationship. We choose to use only ERA5 at this point because it has finer spatial and temporal resolutions than MERRA2, and ERA5 more better represents the diurnal cycle of rainfall over the jet exit region compared to MERRA2 (Fig. 7). Figure 9 shows the correlations found to be statistically significant at the 95% level of confidence after accounting for autocorrelation for TRMM (Fig. 9a), CMORPH (Fig. 9b), IMERG (Fig. 9c), and ERA5 (Fig. 9d)

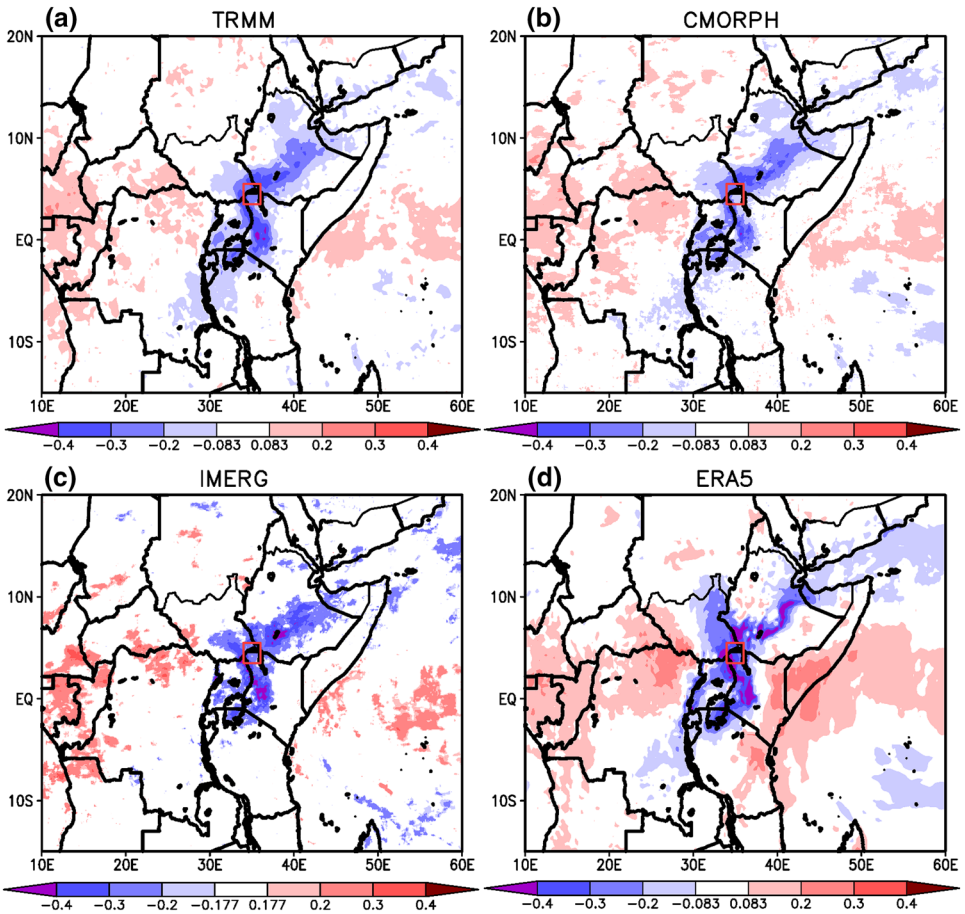

Fig. 9 Correlations between the ERA5 area-averaged 900 hPa daily August wind speed in the Turkana Jet exit region (red box) and daily August precipitation from **a** TRMM, **b** CMORPH, **c** IMERG, and **d** ERA5. **a**–**c** are evaluated from 2000–2017, while **d** is evaluated from 2014–2017. Only values statistically significant at greater than the 95% level of confidence are shaded

daily precipitation. Note IMERG is evaluated over the 2014–2017 period here due to its shorter record length. Furthermore, some caution should be taken when interpreting Fig. 9 because the temporal distribution of daily rainfall can be far from normal, especially in semi-arid to arid regions of Eastern Africa, meaning that the correlations could be skewed. That being said, it is a less of a concern for regions that exhibit larger daily rainfall rates, such as over the South Sudan, which is the focus of this study.

Results from Fig. 9 indicate a robust positive correlation over the Central African Republic and Northern Congo. This pattern is suggestive of a shifting of the active convection center, associated with the Turkana Jet variability. There is also evidence of a positive correlation off the Somali coast in the observations that is more spatially robust in ERA5 (Fig. 9d). While this positive correlation is significant, climatological August monthly rainfall over this region is minimal (Fig. 5), so it is not likely very meaningful at this time of the year.

A significant negative correlation exists between the strength of the Turkana Jet and rainfall over the adjacent Ethiopian Highlands and East African Highlands that seems to follow the East African Rift Valley, in addition to over eastern South Sudan. While it is likely that the variability of the Turkana Jet is directly influencing rainfall variations in the jet exit region of the eastern South Sudan (see Sect. 4.1), a significant relationship also emerges over the adjacent highlands and the jet variability. This suggests that changes in the rainfall/atmospheric conditions over the highlands surrounding the Turkana Channel may be influencing the variability of the jet strength.

To better understand the above-mentioned correlations, composites are formulated based on the strength of the daily Turkana Jet strength index. A strong Turkana Jet day is defined as a day when the jet index is more than 1 standard deviation above the climatological daily mean. Thus, a day is considered a strong jet day when the daily wind speed is greater than 8.70 m s^{-1}. Likewise, a weak jet day is when the index is less than 1 standard deviation below the climatological daily mean, or less than 3.97 m s^{-1}. These identified days are listed in Table 1, and are used to form daily mean (i.e., synoptic) and diurnal cycle composites for the strong and weak jet event types. According to Table 1, there are 112 days that are considered for the strong jet type, and 107 days for the weak jet type. In some instances these days are consecutive.

Also included in Table 1 are counts of the number of events, where an event is defined as the number of

Table 1 ERA5 strong and weak Turkana Jet days used to formulate composites

Year	August Strong jet days	No. of strong jet events	Total no. of strong jet days	August Weak jet days	No. of weak jet events	Total no. of weak jet days
2000	27–29	1	3	7–13, 18, 25	3	9
2001	21, 28	2	2	4, 5, 8, 12, 13, 18	4	6
2002	1, 11–13, 19, 20, 24–30	4	13	7	1	1
2003	4–8	1	5	14–18, 21, 25–28	3	10
2004	4, 28–31	2	5	1, 2, 9–11	2	5
2005	1, 5–8, 11, 12, 28–30	4	10	17, 19–23	2	6
2006	13	1	1	6, 7, 27	2	3
2007	20–22	1	3	1, 11, 16, 17, 29, 30	4	6
2008	12–14	1	3	17	1	1
2009	1, 4–10, 22–31	3	17	–	0	0
2010	1–3, 5–7	2	6	22, 24–26	2	4
2011	1–3	1	3	9–17, 25–29	2	14
2012	–	0	0	1, 8, 13–17, 23–28	4	13
2013	4, 8–10, 24	3	5	14–19	1	6
2014	14, 18, 19	2	3	9, 10, 25–30	2	8
2015	4, 7, 8, 12, 13, 16, 21–29	5	15	1, 19	2	2
2016	12, 14–19, 26–31	3	13	1–5, 21	2	6
2017	3, 4, 16, 20, 21	3	5	7–9, 12, 23, 30, 31	4	7
Total		39	112		41	107

consecutive days when the Turkana Jet index exceeds the defined index threshold for being a strong or weak jet. In some instances an event is just 1 day, while at other times there are multiple days in a row that meet the threshold criterion. Over the 2000–2017 analysis period, there are 39 strong and 41 weak Turkana Jet events. This information is used to conservatively estimate the degrees of freedom when assessing the statistical significance of the composites using a Student's *t* test. Effectively, it helps to better account for autocorrelation between consecutive days in the assessment process rather than use the larger sample sizes based off the total number of days.

4.2.1 Daily mean composite results

Daily means are investigated to provide an overview of the regional synoptic conditions associated with each composite type. Figure 10 shows the precipitation difference from the climatological monthly mean for the strong (Fig. 10a–c) and weak (Fig. 10d–f) Turkana Jet composites using various observational rainfall data and ERA5 output. Results from this analysis indicate that when the Turkana Jet is strong, there is a significant reduction in rainfall over much of South Sudan, the jet exit region west of Lake Turkana, and over the Ethiopian and East African Highlands that flank the Turkana Channel. Meanwhile, further west over eastern Central African Republic and northern Congo there is a significant increase in rainfall. The spatial robustness of the latter is not as coherent as the former at the 95% level of confidence. Conversely, the opposite rainfall anomalies occur for the weak Turkana Jet composites. For both the strong and weak composites, there is strong agreement among the datasets analyzed, including ERA5 precipitation, and the composite results in Fig. 10 are consistent with the Fig. 9 correlations. There is also an anomalous dipole pattern over the tropical and southwestern Indian Ocean.

A variety of fields are next investigated to understand the synoptic and environmental conditions associated with strong and weak Turkana Jet events. Figure 11a shows the ERA5 August climatological 900 hPa geopotential height, while Fig. 11b, c show the 900 hPa geopotential height differences from the climatology for the strong and weak jet composites, respectively. In the climatology (Fig. 11a), there is typically low-level ridging along the East African coastal plain and over the Western Indian Ocean during August. Low-level heights are lower over the continental interior to the west of the Ethiopian and East African Highlands and over continental interior equatorial Africa. For the strong Turkana Jet composite (Fig. 11b), height anomalies are positive over the coastal plain region and western Indian Ocean, and negative to the west of the Highlands, indicating a strengthening of the low-level ridging along coastal East Africa, as well as a deepening of the low-level heights to the west of the topographic barrier. The anomalous low-level geopotential height response is opposite over the western Indian Ocean for the weak Turkana Jet composite (Fig. 11c).

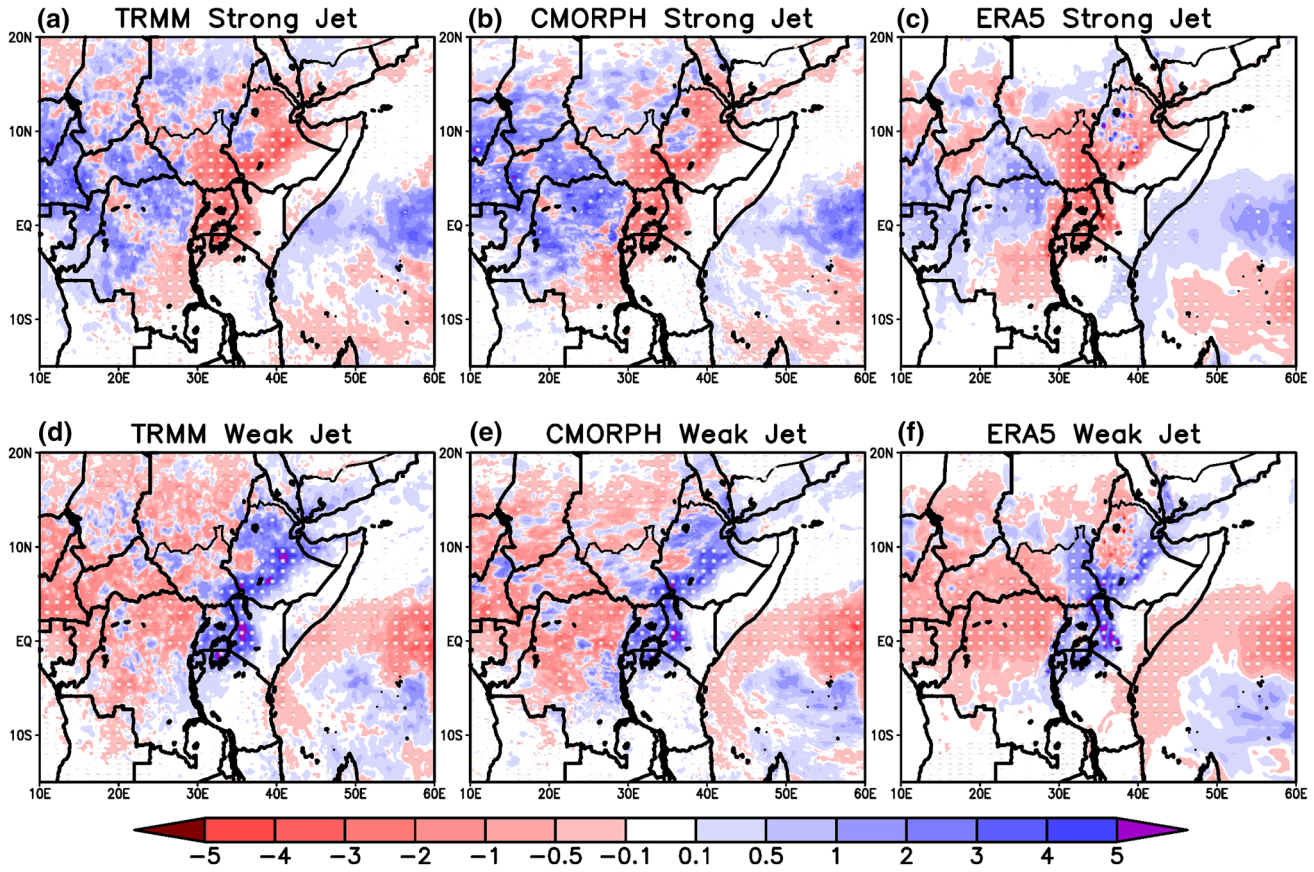

Fig. 10 Strong Turkana Jet composite daily precipitation anomalies (mm day^{-1}) for **a** TRMM, **b** CMORPH, and **c** ERA5. Additionally, weak Turkana Jet composite daily precipitation anomalies for **d** TRMM, **e** CMORPH, and **f** ERA5. Stippling denotes statistically significant values at the 95% level of significance after accounting for autocorrelation

In both the strong and the weak jet cases, the anomalous low-level ridging is found significant at the 95% level of confidence over the coastal plains and western Indian Ocean, but only significant over the equatorial Congo for the strong jet case. Figure 11d shows the climatological August 900 hPa air temperature for reference, while Fig. 11e, f show the strong and weak Turkana Jet composite temperature anomalies. A strong jet is associated with colder low-level temperatures over the western Indian Ocean and East African coastal plain, and warmer low-level temperatures to the west of topographic barrier over Sudan and South Sudan. The cooler conditions are associated with the stronger ridging over the southwestern Indian Ocean (Fig. 11b). Synoptically, these conditions are associated with equatorward moving cold air surges along the high terrain of the East African Highlands that are frequently observed during the austral winter and can last multiple days before moderating (Metz et al. 2013; Crossett and Metz 2017; Hartman 2018). The weak jet composite anomalous temperature pattern is opposite (Fig. 10f), with warming east of the East African and Ethiopian Highlands, and cooling in the Turkana Jet exit region over South Sudan. Subsequently these warmer low-level conditions are consistent with a weakening of the Southern Hemispheric coastal ridging (Fig. 11c).

The climatological August 900 hPa winds are shown in Fig. 11g, while Fig. 11h, i show the strong and weak jet composite anomalous winds. The low-level southeasterly flow is enhanced over the southwest Indian Ocean for the strong jet case, consistent with the anomalous ridging. Over South Sudan, the Central African Republic, and northern Congo, there is anomalous easterly flow (Fig. 11h), indicating a weakening of the low-level southwesterly flow of air from equatorial Congo into the region. This anomalous low-level flow pattern is opposite for the weak jet case (Fig. 11i). Thus, in the weak jet case there is a reduction of the equatorward low-level inflow of relatively cooler extra-tropical/mid-latitude air along the East African coast, and enhanced flow from equatorial Africa into the South Sudan west of the highlands.

These composite low-level circulation differences are also associated with changes in the atmospheric moisture content and instability. Figure 12a shows the ERA5 August climatological precipitable water, while Fig. 12b, c show the precipitable water anomalies for the two composites.

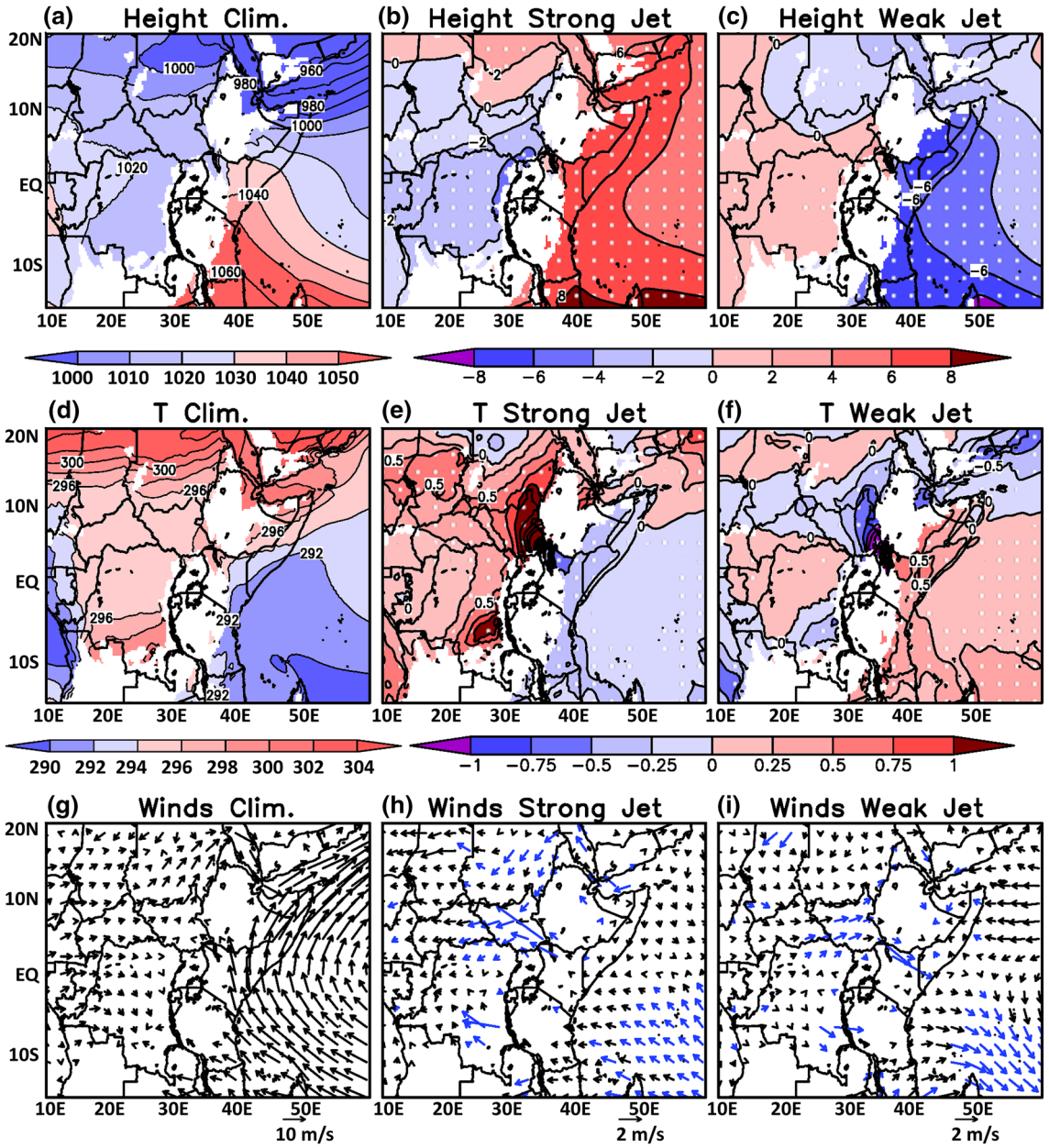

Fig. 11 ERA5 August **a** climatological 900 hPa geopotential heights (m), and 900 hPa geopotential height anomalies for the **b** strong and **c** weak Turkana Jet composites. **d**–**f**, and **g**–**i** are the same as **a**–**c**, but for the ERA5 900 hPa temperatures (K) and 900 hPa winds (m s^{-1}), respectively. Stippling and blue vectors denote values statistically significant at the 95% level of significance after accounting for autocorrelation

The climatology (Fig. 12a) indicates highest precipitable water content occurs to the west of the highlands over the continental interior and equatorial Africa, and not over the western Indian Ocean. South of the equator there is a gradual decrease in precipitable water as one heads poleward, while over the elevated terrain precipitable water content is considerably lower than at sea-level. For the strong jet composite (Fig. 12b), there is a significant reduction in precipitable water over the South Sudan, the Turkana Channel, and the adjacent highlands, and a significant increase in precipitable water over the equatorial Congo basin. Thus, the enhanced, cooler cross-equatorial flow related with the stronger ridging (Fig. 11) is associated with drier conditions in the vicinity of the Turkana Channel, and wetter conditions over equatorial Africa to west of the highlands. This pattern reverses for the weak Turkana Jet composite, with a significant increase (decrease) in precipitable water in the vicinity of the Turkana Channel (over the equatorial Congo basin).

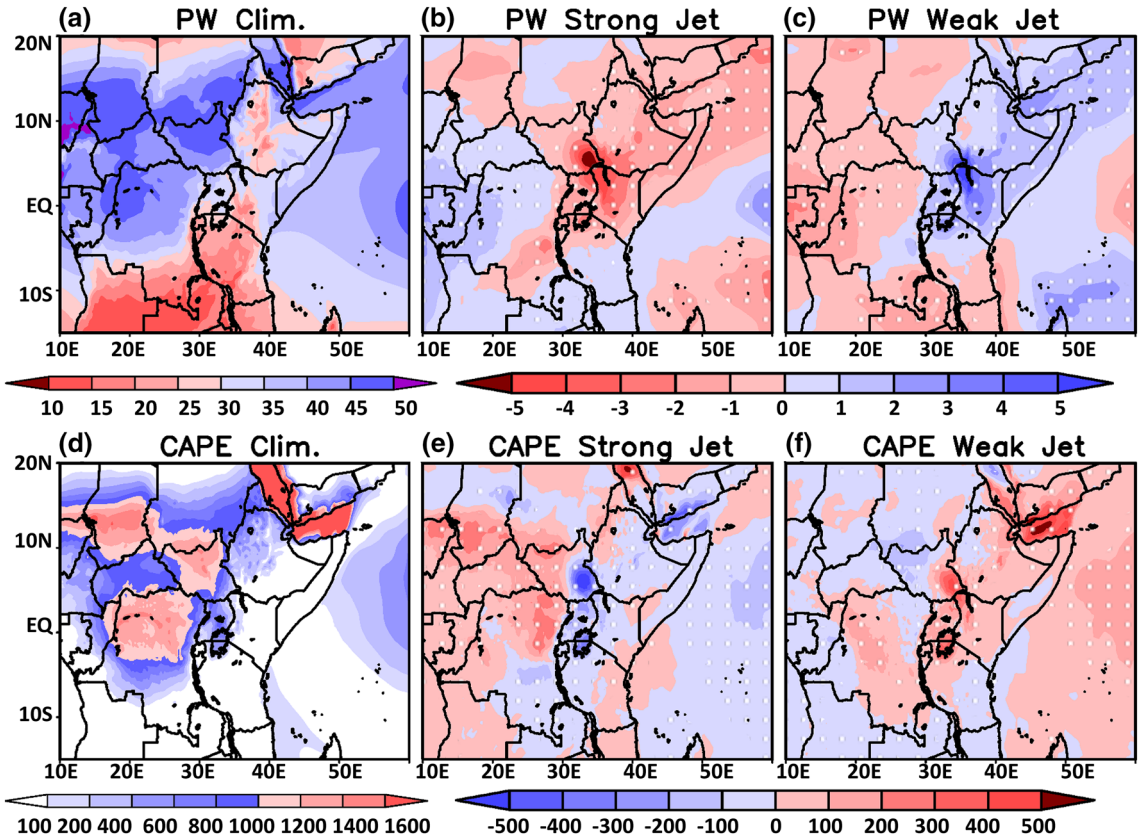

Fig. 12 ERA5 August **a** climatological precipitable water (mm), and precipitable water anomalies for the **b** strong and **c** weak Turkana Jet composites. **d**–**f** are the same as **a**–**c**, but for the ERA5 CAPE (J kg^{-1}). Stippling denote values statistically significant at the 95% level of significance after accounting for autocorrelation

Figure 12d shows the ERA5 climatological August CAPE values, while Fig. 12e, f show the strong and weak jet composite anomalies. In the climatology, the highest values of CAPE are generally found to the west of the highlands over the continental interior. The cooler, drier conditions over the Turkana Channel and South Sudan in the strong jet composite are associated with a significant reduction of CAPE (Fig. 12e); hence, the atmosphere becomes less unstable. Conversely, the warmer, wetter conditions in the vicinity of the Turkana Channel for the weak case are associated with a significant increase in CAPE and a more unstable environment.

4.2.2 Diurnal cycle composite results

Figure 13 shows the diurnal cycle of precipitation averaged between 5°N–6.5°N for the strong and weak Turkana Jet composites from the CMORPH (Fig. 13a, b) and TRMM (Fig. 13c, d) datasets. While rainfall east of 31°E decreases throughout the diurnal cycle for the strong jet composites, we focus now on times when precipitation rates are greater than 4 mm day^{-1} in the climatology (Fig. 6). Compared to the climatology, these heavier rainfall rates drop to less than 2 mm day^{-1} east of 32°E between 00Z–09Z for the strong cases. To the west of 32°E, these heavier rainfall intensities increase to around 15 mm day^{-1} in CMORPH and 25 mm day^{-1} in TRMM between 12Z–21Z compared to the climatology when the jet is strong. Conversely, when the Turkana Jet is weak, rainfall rates generally increase throughout the diurnal cycle. However, focusing on times when there are heavier rainfall rates (> 4 mm day^{-1}) in the climatology indicates that the early morning/daytime heavier rainfall rates increase to the east of 32°E, while late afternoon/evening heavier rainfall rates decrease in CMORPH (Fig. 12b) and TRMM (Fig. 12d).

Figure 14a, b show the ERA5 diurnal cycle of rainfall for the strong and weak jet composites. While not as striking of a decrease as the observations in Fig. 13, ERA5 does capture the reduction of the heavier rainfall rates (e.g., > 4 mm day^{-1}) prior to 12Z east of 32°E, and increase in heavier rainfall rates after 12Z for the strong jet composite (Fig. 14a). For the weak jet composite (Fig. 14b), heavier rainfall rates east of 32°E prior to 12Z intensify compared to the climatology (Fig. 7a). West of 32°E there is still evidence

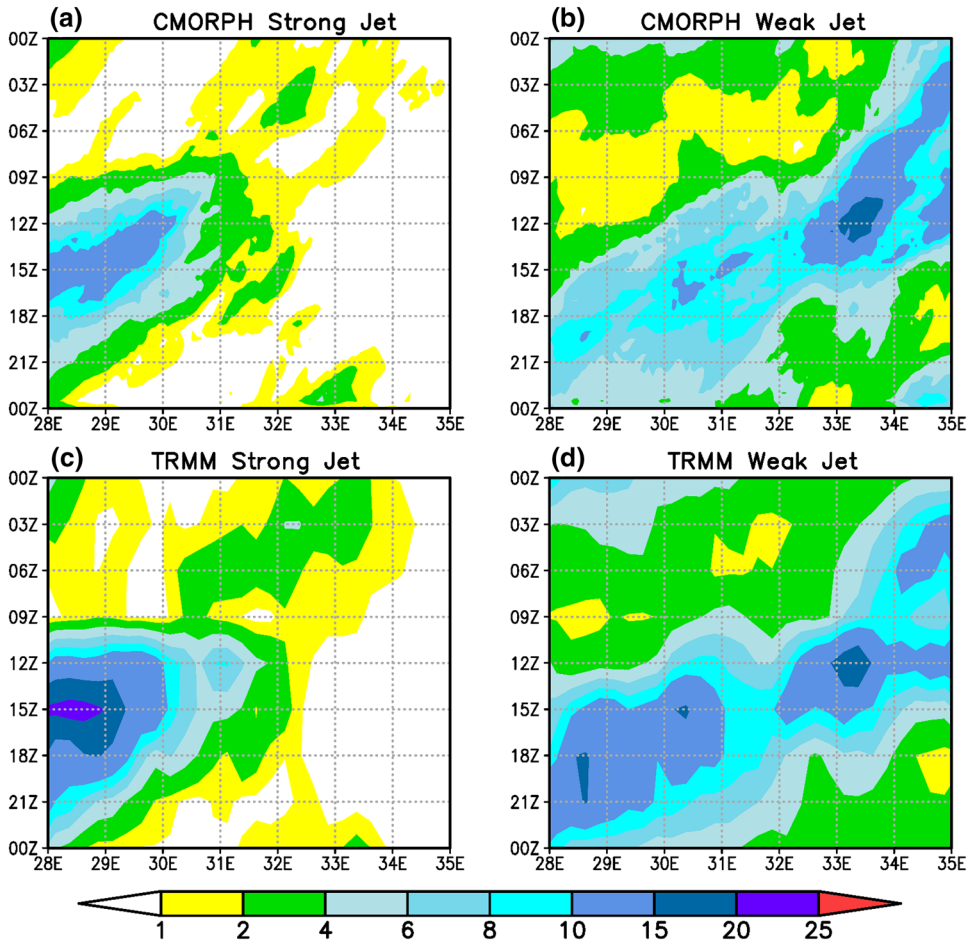

Fig. 13 CMORPH August diurnal cycle of precipitation (mm day^{-1}) averaged between 5°N–6.5°N for the **a** strong and **b** weak Turkana Jet composites. **c**, **d** are the same as **a** and **b**, respectively, but for TRMM

of an afternoon peak in heavier rainfall between 10Z–16Z, however rainfall rates between 17Z–00Z are lower than the climatology (Fig. 7a). This is in contrast to the observations (Fig. 13b, d) which indicate enhanced heavier rainfall over the western South Sudan at this time for the weak jet composite. This suggests that while ERA5 does capture the afternoon development of heavier convection over the western South Sudan, the rain systems are not realistically propagating westward over this region for this composite type under the weaker environmental steering flow. However, this is not an issue for the strong composite case when the environmental steering flow is stronger.

Superimposed on top of the rainfall in Fig. 14a, b are the 900 hPa wind speeds for each composite. The dry conditions east of 32°E over the South Sudan are clearly associated with a stronger Turkana Jet (Fig. 14a) with a peak intensity around 06Z increasing to about 11 m s^{-1} compared to 6 m s^{-1} in the climatology (Fig. 7a). Furthermore, the strong wind speeds penetrate further westward at this time. The jet weakens to around 5–6 m s^{-1} during the daytime between 09Z–18Z, before strengthening once again after 18Z. In contrast, evidence of the Turkana Jet is absent for the weak Turkana Jet case (Fig. 14b) with minimal variation in magnitude.

To relate these diurnal differences in jet strength to the low-level environment, Fig. 14c, d show the diurnal cycle of the 900 hPa wind convergence and specific humidity for the strong and weak jet composites, respectively. In the case of the strong jet, the low-level wind convergence more than doubles compared to the climatology east of 32°E, coinciding with when the jet is strongest during the diurnal cycle, while the low-level moisture content of the atmosphere is 2–3 g kg^{-1} lower than the climatology (Fig. 7c). The stronger Turkana Jet is associated with stronger advection of drier air from the channel further westward into the jet exit region over the eastern South Sudan as evidenced by the lower mixing ratios east of 32°E in Fig. 14c compared to the climatology (Fig. 7c). The lower specific humidity values are associated with an environment that is less unstable despite the clear increase in low-level wind convergence over the region. Thus it is the low-level jet's influence on the atmospheric moisture content that is most important for determining the change in rainfall over the eastern South Sudan for this case.

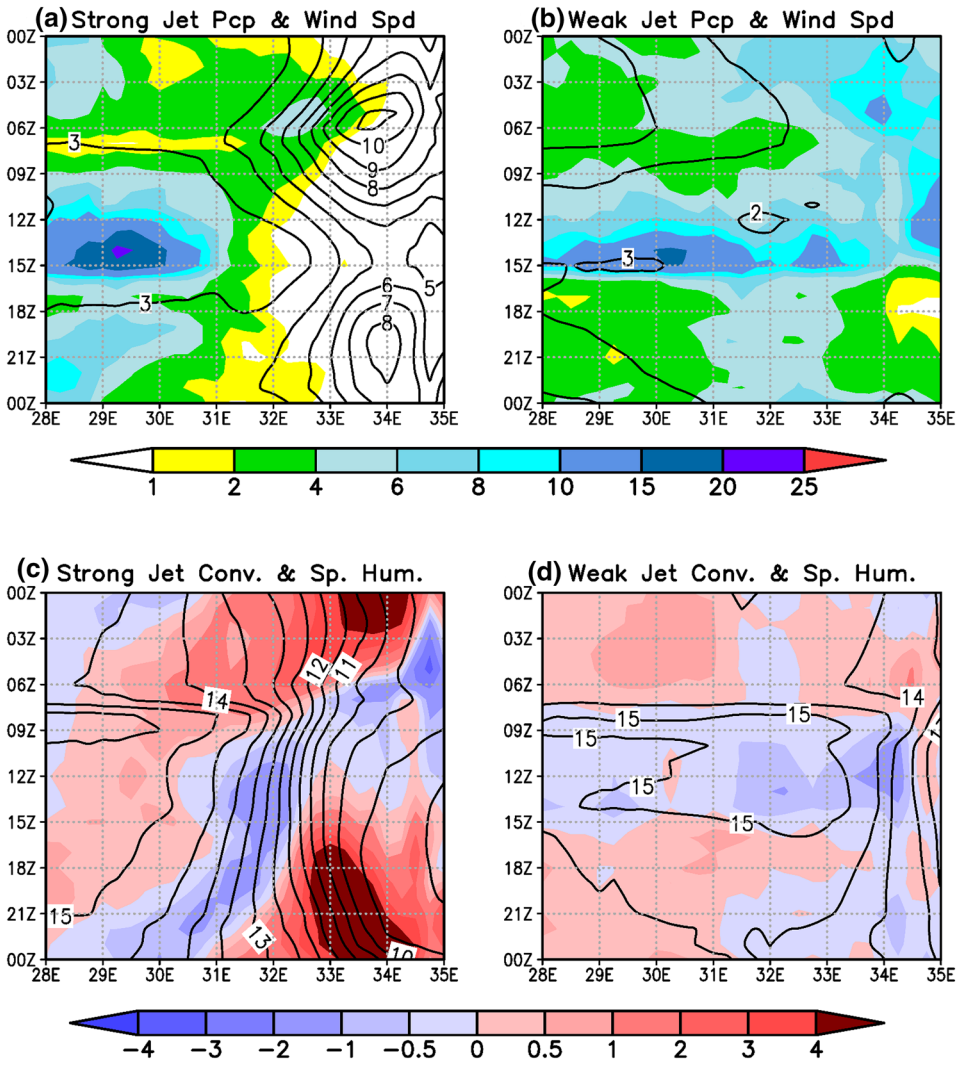

Fig. 14 ERA5 August **a** strong, and **b** weak Turkana Jet composites of the diurnal cycle of precipitation (shaded; mm day^{-1}) and 900 hPa wind speed (contour; m s^{-1}) averaged between 5°N–6.5°N. ERA5 August **c** strong, and **d** weak Turkana Jet composites of the diurnal cycle of 900 hPa wind convergence (shaded; $\times 10^{-5}$ s^{-1}) and the 900 hPa specific humidity (contour; g kg^{-1}) averaged between 5°N–6.5°N

For the weak Turkana Jet case (Fig. 14d), the 900 hPa wind convergence weakens considerably overnight and during the morning compared to the climatology (Fig. 7c). Yet despite this reduction in low-level wind convergence, convective activity increases associated with an increase in the atmospheric moisture content as the low-level specific humidity increases by 2–3 g kg^{-1} over the eastern South Sudan. In this case, the jet weakens considerably west of 36°E resulting in a decrease in transport of relatively drier air during the nighttime and early morning hours. Instead, specific humidity levels remain higher than the climatology, meaning that there is more low-level moisture available that is associated with a more unstable environment as evidenced in the daily mean composite in Fig. 12f. Similar to the strong jet case it is the jet's influence on the atmospheric moisture content, hence atmospheric instability, which appears to be most important for the extent to which convection develops over the eastern South Sudan in the jet exit region.

The next question to address is why exactly is the Turkana Jet is strong or weak for these composites. Recall from our analysis of the daily mean composites of the anomalous low-level 900 hPa flow (Fig. 11h, i), that there is not a statistically significant response in the low level winds over the coastal plains of Kenya and southern Somalia in the Turkana Jet entrance region for either composite case. This indicates that while the synoptic forcing over the region influences the strength of the southeasterly flow north of Madagascar over the southwestern Indian Ocean, it does not appear to directly influence the inflow into the Turkana Channel from the Indian Ocean. This points to the importance of more localized regional processes to explain the significant differences in the Turkana Jet strength.

One such process alluded to in Sect. 4.2.1 when considering the daily/synoptic timescale is the importance of the changes in the Turkana Channel height gradient (i.e., the Bernoulli effect). While difficult to discern from Fig. 11b, c, the channel height gradient is 80% stronger than the

climatology in the strong jet composite, and 70% weaker in the weak jet composite. Almost all (97%) of this intensification of the strong jet channel height gradient is due to the anomalous ridging to the east of the Eastern African topography (Fig. 11b). For the weak jet case however, the decrease in heights to the east of the topography only explains about 70% of change in the channel height gradient (Fig. 11c). Thus, the changes in the synoptic patterns enhances the gradient in the strong jet case, aiding the intensification of the jet. The opposite occurs for the weak jet composite case.

Figure 15a–c show vertical cross sections of the diurnal cycle of the 900 hPa vertical-p velocity and wind speed averaged between 36.5°E–37°E in the center of the Turkana Channel for the climatology, and the strong and weak jet composites, respectively. As indicated in the climatology (Fig. 15a), katabatic downslope flow occurs near the southern channel wall around 2°N from the evening to the morning between 13Z–09Z, with a brief period of rising vertical motions during the afternoon between 09Z–13Z. Similar variations in the diurnal cycle of the vertical motions also occur near the northern wall around 5.5°N with subsidence from around 21Z–06Z, and rising motions during the day. In general, vertical motions adjacent to the northern wall tend to be weaker compared to the southern channel wall as the topographic slope is more gradual relative to the southern wall. Away from the channel walls in the channel between 2.5°N–3°N, and 4°N–4.5°N, the height gradient/pressure drop in the channel is associated with subsidence on the northern and southern flanks of the jet over the entire diurnal cycle. This result is consistent with Hartman (2018), who evaluated a different atmospheric reanalysis (NCEP CFSR) at this time of the year (September). The strength of the subsidence has the same diurnal cycle as the channel height gradient (Fig. 8b) with stronger subsidence during the night, and weaker subsidence during the afternoon hours. That being said, there is not evidence of nighttime

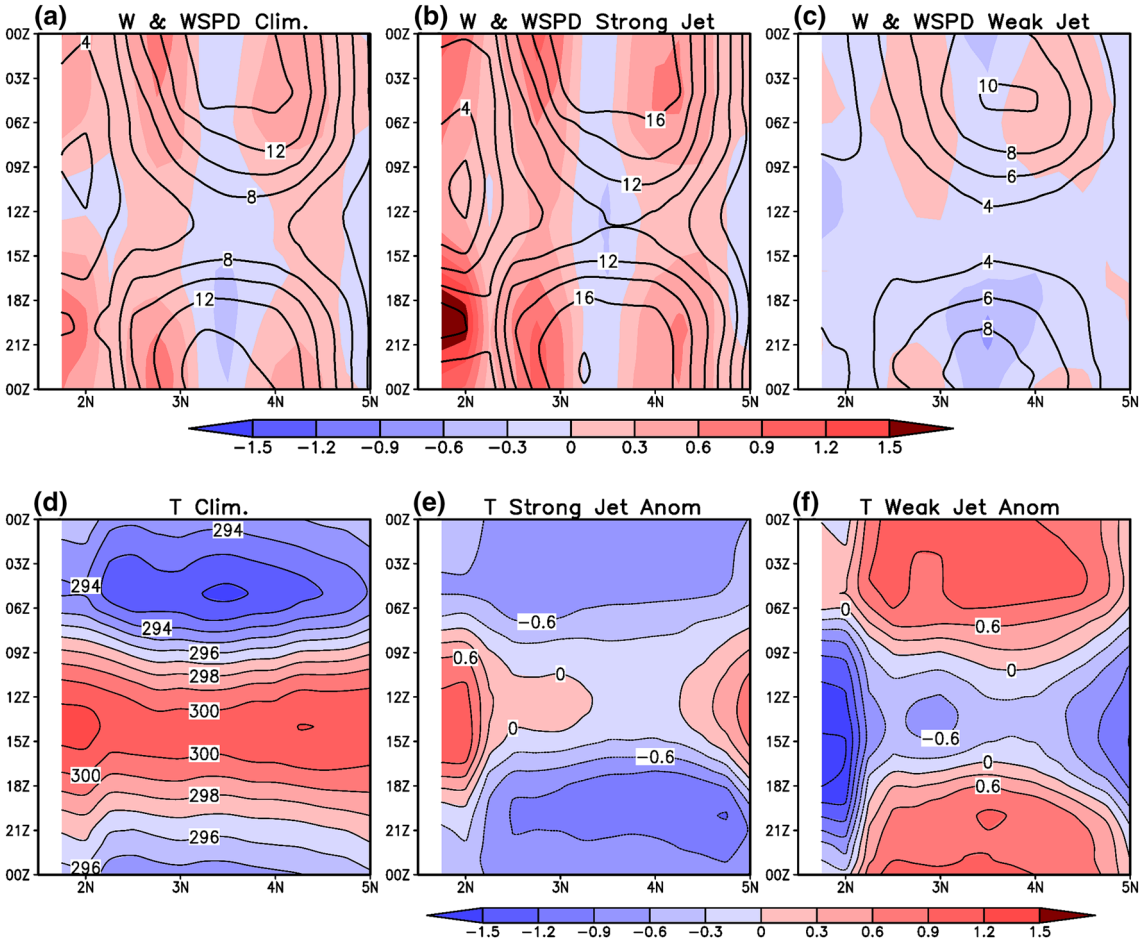

Fig. 15 ERA5 August Turkana Channel diurnal vertical cross-sections of 900 hPa vertical-p velocity (W; shaded; Pa s^{-1}) and wind speed (WSPD; contours; m s^{-1}) averaged between 36.5°E–37°E for the **a** 2000–2017 climatology, and the **b** strong, and **c** weak Turkana Jet composites. **d** ERA5 August diurnal vertical cross-section of temperature (T; shaded and contours; K) for the 2000–2017 climatology as well as the **e** strong and **f** weak Turkana jet composite temperature differences from the climatology. *y* axis is time, while *x* axis is latitude

downslope flow along the channel walls in Hartman's (2018) analysis for September. This difference may be related to the differences in resolution between ERA5 and CFSR (which is 0.5° resolution). For the strong jet composite (Fig. 15b), both the nighttime katabatic downslope flow near the channel walls, particularly the southern wall, and the subsidence associated with the stronger height gradient/pressure drop intensify. Conversely, the vertical motions along the channel walls are upslope at night while the subsidence on the flanks of the jet core weakens when the jet is weak (Fig. 15c).

These changes, in turn, are related to modifications in the temperature field. Figure 15d shows the climatological diurnal cycle of 900 hPa temperature averaged between 36.5°E–37°E for reference, while Fig. 15e, f show the strong jet and weak jet temperature anomaly composites. Results indicate that temperatures are 0.3–0.9 K cooler along the channel walls during the night and early morning, and 0.3–0.9 K warmer during the daytime for the strong jet composite (Fig. 15e). This pattern generally reverses for the weak jet composite (Fig. 15f) with warmer temperatures during the night and early morning, and cooler temperature during the day.

The results of Sect. 4.2.1 and Fig. 15 indicate that the strength of the jet for the composite cases is largely associated with both the synoptic-scale change of the Turkana Channel's low-level height/pressure gradient in addition to changes in the nighttime katabatic flow from the highlands adjacent to the channel. The synoptic conditions associated with a strong Turkana Jet include higher pressure east of the Turkana Channel that enhances the height gradient in the channel, and drier atmospheric conditions in the vicinity of the channel and over the Ethiopian and East African highlands (Fig. 12). During the night, the drier conditions are associated with stronger cooling over the elevated highland slopes adjacent to the Turkana Channel that enhances the nighttime downslope flow into the channel and further strengthens the jet. The opposite occurs for the weak Turkana Jet composite, where synoptic-scale ridging east of the Turkana Channel weakens, reducing the channel height gradient while increasing the atmospheric moisture content in and around the channel. These changes are associated with a weakening of the nighttime cooling over the highlands, hence a decrease in the nighttime katabatic flow into the channel that further weakens the jet. During the day, the synoptic-scale forcing of the height gradient dominates the observed changes in the jet strength for each composite, as the slope flow mechanism becomes less influential. Our findings are consistent with prior studies which have noted the importance of local nighttime katabatic flow for supporting the jet strength (Mukabana and Pielke 1996; Indeje et al. 2001). Furthermore, they help to explain the negative correlations between the jet strength and precipitation over the highlands adjacent to the Turkana Channel, as the same changes in the synoptic and atmospheric environmental conditions that affect the Turkana Jet also influence conditions over the highlands.

5 Summary and conclusions

High-resolution observations and atmospheric reanalyses are analyzed to improve our understanding of the structure and variability of the Turkana Jet, the atmospheric conditions associated with such jet strength variability, and regional rainfall during the peak of the jet exit region's primary wet season (August) on synoptic to diurnal timescales. Fine spatial and temporal resolutions are necessary because the Turkana Channel is narrow in spatial width, and local processes are known to play an important role it influencing the strength of the jet (Mukabana and Pielke 1996; Indeje et al. 2001; Hartman 2018), yet these processes are not as well resolved in coarser resolution observations and atmospheric reanalyses.

A climatological perspective of the relationship is first formulated for the 2000–2017 period by analyzing a variety of high-resolution satellite-derived rainfall datasets (TRMM, CMORPH, and IMERG) and two atmospheric reanalyses (ERA5 and MERRA2). Results from analysis of the satellite-derived rainfall datasets indicate the existence of a distinct diurnal cycle of rainfall over the South Sudan during the wet season (Fig. 6). Over eastern South Sudan east of 32°E, convection is strongest during the late night/ morning hours between 00Z–12Z, and weakest between 15Z and 00Z. Over the western South Sudan west of 32°E, rainfall activity is strongest in the late afternoon and evening hours between 12Z–00Z. Of the two atmospheric reanalyses analyzed, ERA5 better represents this diurnal pattern of rainfall over South Sudan (Fig. 7). This suggests that the higher resolution ERA5, which more realistically represents the topography of Eastern Africa including the Turkana Channel, is likely better suited to understand the relationship between convection over South Sudan and the Turkana Jet during August compared to coarser resolution reanalyses.

Results from the climatological analysis indicate that the Turkana Jet is directly influencing the rainfall over the jet exit region of eastern South Sudan. Enhanced late night/ morning rainfall over the eastern South Sudan is associated with the nighttime intensification of the Turkana Jet (Fig. 7a), which is shown to increase the low-level wind convergence and the strength and location of the low-level zonal moisture gradient over the jet exit region over the eastern South Sudan (Fig. 7c). Overnight when the jet is typically strong, low-level wind convergence in the jet exit region over the eastern South Sudan increases prior to 06Z, which is when the jet extends farthest to the west during the diurnal cycle. The westward extension of the jet between 03Z and

08Z is associated with a brief westward shift of the low-level moisture gradient (Fig. 7c).

The climatological rainfall over the western South Sudan does not appear to be directly influenced by the Turkana Jet. Instead, rainfall over this region appears to be daytime heating-induced late afternoon/evening convection. That being said, there is evidence in the observations (Fig. 6) that suggests morning precipitation systems that spawn over the eastern South Sudan may propagate westward and intensify with daytime heating. However, evidence of this in the ERA5 precipitation field is not as conclusive, as the eastern and western South Sudan precipitation peaks appear to be operating more independent of one another. Further work using higher resolution convection permitting modeling is needed to better understand the extent to which the two rainfall maxima in the diurnal pattern are connected.

Correlations of the daily Turkana Jet strength and daily precipitation indicate that there is a significant negative relationship between the jet strength and rainfall over the Ethiopian and East African Highlands, as well as over the eastern South Sudan (Fig. 9). To investigate the nature of this relationship, daily and diurnal composites are formed for times when the jet is particularly strong and weak.

The daily mean composites, which represent the synoptic timescale, indicate that a strong Turkana Jet is associated with stronger low-level ridging along the coastal plains and adjacent Indian Ocean, primarily south of the equator, accompanied by cooler and drier conditions that infiltrate over the highlands and into the Turkana Channel (Fig. 11). Such conditions are consistent with the equatorward advance of cold air surges to the east of the topographic barrier that are known to occur during the austral winter (Metz et al. 2013; Crossett and Metz 2017; Hartman 2018). The stronger ridging enhances the height/pressure gradient in the channel leading to a stronger jet as explained by the Bernoulli effect (Indeje et al. 2001). Conversely, a weak Turkana Jet is associated with weaker low-level ridging along the coastal plains and adjacent Indian Ocean, a weakening of the Turkana channel height/pressure gradient, hence Bernoulli effect, and warmer, and wetter atmospheric conditions that aid in destabilizing the atmosphere over the eastern South Sudan (Fig. 12). This is interpreted here as the influence of a more tropical air mass regime.

Analysis of the composite days at diurnal timescales indicates that the cooler and drier conditions associated with a stronger Turkana Jet, are also associated with an amplification of the diurnal cycle of the jet (Fig. 14). The drier atmospheric conditions promote stronger cooling at night over the highlands adjacent to the Turkana Channel resulting in enhanced katabatic flow into the channel that further drives the strong jet (Fig. 15). The opposite occurs for the weak Turkana Jet case, as the warmer and more moist atmospheric conditions over the channel and adjacent highlands are conducive to weaker nighttime cooling and reduced katabatic flow into the channel, resulting in the further weakening of the jet.

Finally, a few conclusions can be drawn from our analysis. They are:

- When comparing results from the climatological mean state (Sect. 4.1) and the strong and weak jet composites (Sect. 4.2) there is an apparent contradiction in the relationship between eastern South Sudan rainfall in the jet exit region and the Turkana Jet strength. Analysis of the climatological mean diurnal cycle indicates that rainfall is enhanced in the early morning hours when the Turkana Jet is strongest (Figs. 5, 6), but an opposite relationship is found when the days are more carefully selected to form strong and weak jet composites (Figs. 13, 14). This contradiction is an artifact of the methodology used to process the datasets, as the climatological analysis considers all types of events including periods when the jet is weak and rainfall is enhanced over the jet exit region, and strong jet periods when the convection is suppressed in the jet exit region. Averaging all types of events together obscures the relationship between the jet strength and rainfall in the jet exit region. Utilizing a compositing approach to separate strong and weak jet periods yields a more complete understanding of this relationship.
- The Turkana Jet strength itself appears to be strongly influenced by variations in the heating/cooling over the adjacent Ethiopian and East African Highlands, which is consistent with past studies (Indeje et al. 2001; Hartman 2018). Furthermore, while synoptically-forced changes by the large-scale circulation/atmospheric conditions are important, they can also manifest themselves to further influence the strength of the Turkana Jet via their modulation on the katabatic flow within the Turkana Channel, with cooler and drier conditions associated with a stronger jet, and vice versa. Hence, this may help to explain the significant negative correlations between the Turkana Jet strength and environmental fields such as precipitation over the highlands (Fig. 9).
- It is the Turkana jet's influence on the atmospheric moisture content rather than its impact on low-level convergence over the jet exit region of South Sudan that appears to be most important during the boreal summer. When the jet is strong, enhanced low-level wind convergence over the exit region does not translate into increased rainfall because the air is relatively dry and less unstable at this time of the year. Conversely, a weaker jet is associated with weaker wind convergence, but the low-level moisture content is enhanced resulting in greater atmospheric instability that favors convection over the eastern South Sudan.

- During the boreal summer, synoptic variability of the Turkana Jet and South Sudan rainfall appears to be closely associated with the strength of low-level ridging along the East African coast south of the equator and over the southwestern Indian Ocean. That being said, this study did not find any statistically significant evidence that stronger ridging directly results in enhanced inflow into the Turkana Jet entrance region diverted from the cross-equatorial low-level jet (e.g., the Somali Jet). Instead, the influence of the ridging on the jet strength is manifested through its control on the low-level height gradient in the Turkana Channel as explained by the Bernoulli effect (Indeje et al. 2001). This suggests that the synoptic variability not directly, but indirectly may influence rainfall via its impact on the atmospheric conditions (e.g., temperature, atmospheric moisture content, stability) over the Turkana Channel and the adjacent highlands. The robustness of this conclusion still needs to be more rigorously evaluated as this study focuses on results obtained from analyzing a single atmospheric reanalysis, ERA5.
- The findings here demonstrate the importance of realistically representing the smaller-scale processes important for influencing variations in the Turkana Jet. While some knowledge of the Turkana Jet variability may be obtained from analyzing coarser resolution atmospheric reanalyses (Nicholson 2016), it may not yield a complete understanding of the rainfall variations in the jet exit region of eastern South Sudan because of the influence of these more localized processes. Our next step is to evaluate the robustness of our findings in this study using convection permitting modeling at spatial resolutions less than 4-km.

Acknowledgements This work was funded by NSF Award #1701520. The authors acknowledge the Texas Advanced Computing Center (TACC) at The University of Texas at Austin for providing HPC and database resources that have contributed to the research results reported within this paper. URL: http://www.tacc.utexas.edu. The Grid Analysis and Display System software (GrADS) developed at COLA/IGES was used for generating the figures. The authors would like to thank Declan Finney and the anonymous reviewer for their constructive comments and suggestions.

References

Anderson DLT (1976) The low-level jet as a westerm boundary current. Mon Weather Rev 104:907–921. https://doi.org/10.1175/1520-0493(1976)104%3c0907:TLLJAA%3e2.0.CO;2

Bannon PR (1979) On the dynamics of the East African Jet. I: simulation of mean conditions for July. J Atmos Sci 36:2139–2152. https://doi.org/10.1175/1520-0469(1979)036%3c2139:OTDOTE%3e2.0.CO;2

Bunker AF (1965) Interaction of the summer monsoon air with the Arabian Sea. In: Proceedings of the symposium on meteorological results of t I.I.O.E., Bombay, 22–26 July 1965. Poona, Indian Meteorological Department, pp 3–16

Cook KH, Vizy EK (2012) Impact of climate change on mid-21st century growing seasons in Africa. Clim Dyn 39:2937–2955. https://doi.org/10.1007/s00382-012-1324-1

Cook KH, Vizy EK (2013) Projected changes in East African rainy seasons. J Clim 26:5931–5948. https://doi.org/10.1175/JCLI-D-12-00455.1

Crossett CC, Metz ND (2017) A climatological study of extreme cold surges along the African Highlands. J Appl Meteorol Climatol 56:1731–1738. https://doi.org/10.1175/JAMC-D-15-0191.1

Dee DP, Uppala SM, Simmons AJ et al (2011) The ERA-Interim reanalysis: configuration and performance of the data assimilation system. Q J R Meteorol Soc 137:553–597. https://doi.org/10.1002/qj.828

Dezfuli AK, Ichoku CM, Huffman GJ, Mohr KI, Selker JS, van de Giesen N, Hochreutener R, Annor FO (2017) Validation of IMERG precipitation in Africa. J Hydrometeorol 18:2817–2825. https://doi.org/10.1175/JHM-D-17-0139.1

ERA5 (2018) Generated using Copernicus Climate Change Service Information 2018. Neither The European Commission nor ECMWF is responsible for any use that may be made of the Copernicus Information of Data it contains. http://apps.ecmwf.int/data-catalogues/era5/?class=ea

Findlater J (1966) Cross-equatorial jet streams at low level over Kenya. Meteorol Mag 95:353–364

Findlater J (1969) A major low level air current near the Indian Ocean during the northern summer. Q J R Meteorol Soc 95:362–380. https://doi.org/10.1002/qj.49709540409

Findlater J (1977) Observational aspects of the low-level cross-equatorial jet stream of the western Indian Ocean. Pageoph 115:1251–1262. https://doi.org/10.1007/BF00874408

Funk C, Peterson P, Landsfeld M, Pedreros D, Verdin J, Shukla S, Husak G, Rowland J, Harrison L, Hoell A, Michaelsen J (2015) The climate hazards infrared precipitation with stations—a new environmental record for monitoring extremes. Sci Data 2:150066. https://doi.org/10.1038/sdata.2015.66

Gelaro R, McCarty W et al (2017) The modern-era retrospective analysis for research and applications, version 2 (MERRA-2). J Clim 30:5149–5454. https://doi.org/10.1175/JCLI-D-16-0758.1

Griffith JF (1972) Climate Survey of Africa, vol 10. World Survey of Climatology,m Elsevier, Amsterdam, p 604

Hart JE (1977) On the theory of the East African low level jet stream. Pageoph 115:1263–1282. https://doi.org/10.1007/BF00874409

Hart JE, Rao GV, Boogaard HVD, Young JA, Findlater J (1978) Arieal observations of the East African low-level jet stream. Mon Weather Rev 106:1714–1724. https://doi.org/10.1175/1520-0493(1978)106%3c1714:AOOTEA%3e2.0.CO;2

Hartman AT (2018) An analysis of the effects of temperatures and circulations on the strength of the low-level jet in the Turkana Channel in East Africa. Theor Appl Climatol 132:1003–1017. https://doi.org/10.1007/s00704-017-2121-x

Herrmann SM, Mohr KI (2011) A continental-scale classification of rainfall seasonality regimes in Africa based on gridded precipitation and land surface temperature products. J Appl Meteorol Climatol 50:2504–2513. https://doi.org/10.1175/JAMC-D-11-024.1

Huffman GJ, Adler RF, Bolvin DT, Gu G, Nelkin EJ, Bowman KP, Hong Y, Stocker EF, Wolff DB (2007) The TRMM multisatellite precipitation analysis (TMPA): quasi-global, multiyear, combined-sensor precipitation estimates at fine scales. J Hydrometeorol 8:38–55. https://doi.org/10.1175/JHM560.1

Huffman G, Bolvin D, Braithwaite, Hsu K, Joyce R, Xie P (2014) Integrated Multi-satellitE Retrievals for GPM (IMERG), version 4.4. NASA's Precipitation Processing Center. ftp://arthurhou.pps.eosdis.nasa.gov/gpmdata. Accessed 1 June 2018

Indeje M, Semazzi FHM, Xie L (2001) Mechanistic model simulations of the East African climate using NCAR regional climate model: influence of large-scale orography on the Turkana low-level jet. J Climate 14:2710–2724. https://doi.org/10.1175/1520-0442(2001)014%3c2710:MMSOTE%3e2.0.CO;2

Joyce R, Janowiak J, Arkin PA, Xie P (2004) CMORPH: a method that produces global precipitation estimates from passive microwave and infrared data at high spatial and temporal resolution. J Hydrometeor 5:487–503. https://doi.org/10.1175/1525-7541(2004)005%3c0487:CAMTPG%3e2.0.CO;2

Kinuthia JH (1992) Horizontal and vertical structure of the Lake Turkana Jet. J Appl Meteorol 31:1248–1274. https://doi.org/10.1175/1520-0450(1992)031%3c1248:HAVSOT%3e2.0.CO;2

Kinuthia JH, Asnani GC (1982) A newly found jet in North Kenya (Turkana Channel). Mon Weather Rev 110:1722–1728. https://doi.org/10.1175/1520-0493(1982)110%3c1722:ANFJIN%3e2.0.CO;2

Kobayashi S, Ota Y, Harada Y, Ebita A, Moriya M, Onogi K, Kamahori H, Kobayashi C, Endo H, Miyaoka K, Takahashi K (2015) The JRA-55 reanalysis: general specifications and basic characteristics. J Meteorol Soc Jap 93:5–48. https://doi.org/10.2151/jmsj.2015-001

Krishnamurti TN, Molinari J, Pan H-L (1976) Numerical simulation of the Somali Jet. J Atmos Sci 33:2350–2362. https://doi.org/10.1175/1520-0469(1976)033%3c2350:NSOTSJ%3e2.0.CO;2

Levin NE, Zipser EJ, Cerling TE (2009) Isotopic composition of waters from Ethiopia and Kenya: insights into moisture sources for eastern Africa. J Geophys Res 114:D23306. https://doi.org/10.1029/2009JD012166

Liebmann B, Hoerling MP, Funk C, Bladé I, Dole RM, Allured D, Quan X, Pegion P, Eischeid JK (2014) Understanding recent eastern Horn of Africa rainfall variability and change. J Clim 27:8630–8645. https://doi.org/10.1175/JCLI-D-13-00714.1

Lu J (2018) 'Unimaginable' suffering in south Sudan. Is there any hope? In: NPR. https://www.npr.org/sections/goatsandsoda/2018/07/05/620184859/unimaginable-suffering-in-south-sudan-is-there-any-hope. Accessed 12 Dec 2018

Lyon B, DeWitt DG (2012) A recent and abrupt decline in the East African long rains. Geophys Res Lett 39:L02702. https://doi.org/10.1029/2011GL050337

Mekonnen A, Thorncroft CD (2016) On mechanisms that determine synoptic time scale convection over East Africa. Int J Climatol 36:4045–4057. https://doi.org/10.1002/joc.4614

Mekonnen A, Thorncroft CD, Aiyyer AR, Kiladis G (2008) Convectively coupled Kelvin waves over tropical Africa during the boreal summer: structure and variability. J Clim 21:6649–6667. https://doi.org/10.1175/2008JCLI2008.1

Metz ND, Archambault HM, Srock AF, Galarneau TJ Jr, Bosart LF (2013) A comparison of South American and African preferential pathways for extreme cold events. Mon Weather Rev 141:2066–2086. https://doi.org/10.1175/MWR-D-12-00202.1

Mukabana JR, Pielke RA (1996) Investigating the influence of synoptic-scale monsoonal winds and mesoscale circulations on diurnal weather patterns over Kenya using a mesoscale numerical model. Mon Weather Rev 124:224–242. https://doi.org/10.1175/1520-0493(1996)124%3c0224:ITIOSS%3e2.0.CO;2

Ngara T, Asnani GC (1978) Five-day oscillation in East African low-level jet. Nature 272:708–709. https://doi.org/10.1038/272708a0

Nicholson SE (1996) A review of climate dynamics and climate variability in eastern Africa. In: Johnson TC, Odada EO (eds) The limnology, climatology and paleoclimatology of the East African Lakes. Gordon and Breach, Toronto, pp 25–56

Nicholson SE (1998) Historical Fluctuations of Lake Victoria and Other Lakes in the Northern Rift Valley of East Africa. In: Lehman JT (eds) Environmental change and response in East African Lakes. Monographiae Biologicae, vol 79. Springer, Dordrecht. https://doi.org/10.1007/978-94-017-1437-2_2

Nicholson SE (2000) The nature of rainfall variability over Africa on times scales of decades to millennia. Glob Planet Change 26:137–158. https://doi.org/10.1016/S0921-8181(00)00040-0

Nicholson SE (2016) The Turkana low-level jet: mean climatology and association with regional aridity. Int J Climatol 36:2598–2614. https://doi.org/10.1002/joc.4515

ReliefWeb (2017) Republic of South Sudan: current and projected (January–July 2017) Acute Food Insecurity Situation—South Sudan. In: ReliefWeb https://reliefweb.int/report/south-sudan/republic-south-sudan-current-and-projeted-january-jul-2017-acute-food. Accessed 12 Dec 2018

Riddle EE, Cook KH (2008) Abrupt rainfall transitions over the Greater Horn of Africa: observations and regional model simulations. J Geophys Res 113:D15109. https://doi.org/10.1029/2007JD009202

Rodwell MJ, Hoskins BJ (1995) A model of the Asian summer monsoon. Part II: cross-equatorial flow and PV behavior. J Atmos Sci 52:1341–1356. https://doi.org/10.1175/1520-0469(1995)052%3c1341:AMOTAS%3e2.0.CO;2

Rowell DP, Booth BBB, Nicholson SE, Good P (2015) Reconciling past and future rainfall trends over East Africa. J Climate 28:9768–9788. https://doi.org/10.1175/JCLI-D-15-0140.1

Sun L, Semazzi FHM, Giorgi F, Ogallo L (1999) Application of the NCAR regional climate model to eastern Africa 1. Simulation of the short rains of 1988. J Geophys Res 104:6529–6548. https://doi.org/10.1029/1998JD200051

Trewartha GT (1981) The Earth's problem climates. University of Wisconsin Press, Madison, p 340

Williams AP, Funk C, Michaelsen J, Rauscher SA, Robertson I, Wils THG, Koprowski M, Eshetu Z, Loader NJ (2012) Recent summer precipitation trends in the Greater Horn of Africa and the emerging role of Indian Ocean sea surface temperature. Clim Dyn 39:2307–2328. https://doi.org/10.1007/s00382-011-1222-y

Xie P, Joyce R, Wu S, Yoo S-H, Yarosh Y, Sun F, Lin R (2017) Reprocessed, biased-corrected CMORPH global high-resolution precipitation estimates from 1998. J Hydrometeorol 18:1617–1641. https://doi.org/10.1175/JHM-D-16-0168.1